Human primary liver cancer–derived organoid cultures for disease modeling and drug screening

Tumour-derived Organoid Cultures model Primary Human Liver Cancer *in vitro*

Laura Broutier[1], Gianmarco Mastrogiovanni#[1,3], Monique M.A. Verstegen#[2], Hayley E. Francies#[4], Lena Morrill Gavarró[3], Charles R Bradshaw[1], George E Allen[1], Robert Arnes[1], Marcia P. Gaspersz[2], Nikitas Georgakopoulos[5], Bon-Kyoung Koo[3], Sabine Dietman[3], Susan E. Davies[6], Raaj K. Praseedom[7], Ruby Lieshout[2], Jan N. M. IJzermans[2], Stephen J Wigmore[8], Kourosh Saeb-Parsy[5], Mathew J. Garnett[4], Luc J.W. van der Laan[2], Meritxell Huch[1,3,9*]

(1) The Wellcome Trust/CRUK Gurdon Institute, University of Cambridge, UK.
(2) Department of Surgery, Erasmus MC-University Medical Center, Rotterdam, Netherlands.
(3) Wellcome Trust - Medical Research Council Stem Cell Institute, University of Cambridge, UK.
(4) Wellcome Trust Sanger Institute, Wellcome Trust Genome Campus, Hinxton, UK.
(5) Department of Surgery, University of Cambridge and NIHR Cambridge Biomedical Research Centre, Cambridge, UK.
(6) Department of Histopathology, Cambridge University Hospitals NHS Foundation Trust, Cambridge, UK.
(7) Department of Pancreatico-hepatobiliary Surgery, Cambridge University Hospitals NHS Foundation Trust, Cambridge, UK.
(8) Department of Clinical Surgery, Royal Infirmary of Edinburgh, Edinburgh, UK.
(9) Department of Physiology, Development and Neuroscience, University of Cambridge, Cambridge, UK.
# equal contribution
*correspondence: m.huch@gurdon.cam.ac.uk

Abstract

Human liver cancer research currently lacks *in vitro* models that faithfully recapitulate the pathophysiology of the original tumour. We recently described a novel, near-physiological organoid culture system, where primary human healthy liver cells form long-term expanding organoids that retain liver tissue function and genetic stability. Here, we extend this culture system to the propagation of primary liver cancer (PLC) organoids from three of the most common PLC subtypes: hepatocellular carcinoma (HCC), cholangiocarcinoma (CC) and combined HCC/CC (CHC) tumours. PLC-derived organoid cultures preserve the histological architecture, gene expression and genomic landscape of the original tumour, allowing discrimination between different tumour tissues and subtypes, even after long term expansion in culture in the same medium conditions. Xenograft studies demonstrate that the tumourogenic potential, histological features and metastatic property of PLC-derived organoids are preserved *in vivo*. Furthermore, PLC-derived organoids prove useful in identifying novel genes involved in liver cancer progression, such as *C1QBP* (for CC) and *C19orf48* (for HCC), and are amenable for drug screening, thus facilitating the identification of the ERK inhibitor SCH772984 as a potential therapeutic agent for liver cancer. We thus demonstrate the wide-ranging biomedical utilities of PLC-derived organoid models in furthering the understanding of liver cancer biology and in developing drug screening platforms for liver cancer personalized medicine approaches.

Primary liver cancer (PLC) represents a major health problem [1]. It is the second most common malignancy worldwide in terms of mortality, and incidence rates are rising, mainly due to an increase in associated risk factors such as diabetes and obesity [2, 3]. Primary liver cancer is generally classified into either hepatocellular carcinoma (HCC) or cholangiocarcinoma (CC), with the majority of all primary liver tumours falling into one of these two categories [1]. Also, a combined hepatocellular-cholangiocarcinoma (CHC), accounting for 0.4 to 14.2% of all PLCs [4] harbours intermediate characteristics between HCC and CC [5]. Albeit both, HCC and CC are easily distinguishable by their histological appearance [3, 5] and genetic and transcriptional landscapes [6], with CHC sharing histological features of both [7], PLC is overall a complex entity, which renders each case of the disease unique and in need of precise and personalized treatment approaches.

The development of effective treatments for liver cancer has been hindered by the shortage of reproducible human models to assess the efficacy of candidate therapeutic agents [8]. Historically, preclinical models have mainly consisted of genetically engineered mouse models or of human tumour-derived cell lines propagated in either 2D-culture or as xenografts in mice [8-10]. While 2D-culture has allowed pioneering advances in cancer cell and molecular biology, it fails to recapitulate critical features of a growing tumour *in vivo* [11]. These include the 3D organization of cells as well as cell-cell and cell-matrix interactions within the tumour. In addition, PLC, especially CCs, have proven difficult to propagate *in vitro*, with only 2 cell lines reported thus far [12, 13].

There has been recent emergence of *in vitro* culture systems of primary, non-transformed tissues growing as 3D structures, termed organoids, which accurately recapitulate tissue architecture and function. Organoids have opened up avenues to study human physiology and disease in an unprecedented manner [14]. Thus retinal, cerebral, kidney, intestinal and stomach organoids (among others) have already been generated from pluripotent stem cells for the study of human development and disease *ex vivo* [15]. In addition, organoids are promising disease models not only for understanding the biology of human diseases but also for testing drug efficacy *in vitro*, before moving to animal models. Notably, however, the study of human cancer, a disease of adult somatic cells, requires the establishment of culture systems directly from patient material as opposed to pluripotent stem cells. Accordingly, mouse and human cancer organoids have recently been established for colon [16-18], pancreas [16, 19] and prostate [20] tumours, but not, thus far, from liver tumours.

Based on our previous work in mouse liver and pancreas organoid cultures [21, 22], we recently showed that organoid cultures derived from human liver donor/healthy biopsies could be expanded long-term *in vitro* while preserving their liver functionality and genetic stability over time [23]. Here, we demonstrate the proof-of-concept that liver organoid cultures also recapitulate human primary liver cancer *in vitro*. Hence, we have successfully established organoid cultures from 8 PLC patients, encompassing three of the most common subtypes of primary liver cancer [1]: HCC, CC and CHC. PLC-derived organoids recapitulate the histological architecture, expression profile, genomic landscape and *in vivo* tumourigenesis of the parent tumour, even after long-term expansion in culture. In addition, we demonstrate the utility of PLC-derived organoids for identifying novel genes potentially involved in liver cancer progression and potential novel therapeutic targets, thus opening up opportunities for drug testing and advances in personalized medicine approaches.

RESULTS

Tumour-derived human primary liver cancer organoids expand long-term *in vitro* while preserving the histological architecture and marker expression of the specific tumour subtype they derive from.

By adapting our previous protocol to isolate and expand murine adult liver stem/progenitor cells [22], we have recently established culture conditions for the long-term expansion of human cells derived from liver donor/healthy biopsies [23, 24]. Here, we sought to selectively expand tumour cells from human PLC tissue by optimizing our established human liver expansion protocol. Surgically resected liver tumour tissue was obtained from untreated PLC patients who had no history of viral-meditated hepatitis (excluded under Institutional safety guidelines). The specimens were assessed for routine histological diagnostic and staging requirements prior to tissue being taken for organoid derivation, part of this tissue also being retained and preserved for genomic, transcriptomic and histological analyses. The remainder was dissociated and processed for culturing (Fig. 1a). We observed that normal/healthy contaminating tissue within the samples gave rise to organoids that would quickly outcompete the tumour-derived organoids, presumably due to differences in genetic stability, as previously reported for colon cancer [18]. Therefore, to avoid the growth of healthy contaminating organoids, we modified our derivation protocol by (i) adapting the timing of tissue digestion, (ii) changing the starting culture conditions using, in addition of the classical isolation medium for healthy liver-derived organoid culture [23, 24], a newly defined PLC-derived organoids isolation medium consisting in the classical expansion medium for healthy liver-derived organoids [23, 24] without Rspo1 and supplemented with 3nM Dexamethasone and Y27632 (Fig. 1c) and (iii) closely monitoring the developing organoid structures (see Suppl. Fig. 1 + methods for details).

Using this novel protocol, we successfully established human PLC-derived organoids from 8 different PLC patients, including poorly to moderate-to-well differentiated HCC (n=3) and CC (n=3), and combined HCC/CC (CHC; n=2) (Fig. 1, Suppl. Fig. 2a and Suppl. Table 1). We found a strong correlation between the derivation success rate (establishment) and the proliferation index of the original tumour. Thus, we successfully established organoid cultures from 100% of the samples derived from tumours that contained > 5% proliferating cells, while we did not succeed in deriving material from very well differentiated lesions, with <5% proliferative cells in the original samples, in agreement with the histological grading of early HCCs [5] (Suppl. Fig. 2b-g and Suppl. Table 1). Of note, after the first derivation, all cultures, irrespective of their subtype-of-origin, were maintained in the same culture conditions as our already defined human healthy liver-derived organoid complete medium [23, 24] (see methods for details).

PLC-derived organoids (also termed “tumouroids” from hereon) from all 3 different subtypes expanded long-term (~1year) in culture (Fig. 1d and Suppl. Fig. 2h), with a consistent passaging ratio of 1:3-1:4 every 7-10 days (Fig. 1d). HCC-2, though, stopped growing after 1.5 months (passage 3), due to the presence of fibroblasts in the culture, which outcompeted the tumouroids growth and precluded any downstream analysis (Fig. 1d). Therefore, we have performed all the downstream analysis on the remaining 7 lines and corresponding patient’s tissues (HCC-1 and -3; CHC-1 and -2 and CC-1, -2 and -3).

At the histological level, tumouroids presented patient-specific heterogeneous morphologies ranging from very solid, compact structures (HCC and CHC) to more irregularly-shaped cyst-like structures (CC) in contrast to the ordered, homogeneous, cyst-like hollow structure of

healthy liver-derived organoids (Fig. 1b and Suppl. Fig. 2a). These morphological features allowed individual samples to be distinguished from each other, both within and between tumour subtypes, even at late passage and after having been cultured in the same medium conditions (Suppl. Fig. 2h). Also, successfully expanded tumouroids could be readily frozen and thawed, without affecting their morphological structure or expansion potential, using our previously described protocol [24].

We then sought to determine whether the 3D-tumouroids would retain the histological features of the original patient tumour tissue. Healthy liver-derived organoids form single-layered epithelial structures (Fig. 1b) that transition into a pseudo-stratified epithelium upon differentiation (see [23] for details). In contrast, the tumouroids exhibited a very different histological and cellular architecture, which recapitulated the histological features of the patient's tissue and tumour subtype (Fig. 1b and Suppl. Fig. 2a). Thus, HCC and CHC tumouroids exhibited a solid, filled 3D structure with HCCs but not CHCs also forming pseudoglandular rosettes, a typical pattern of HCC [1, 7]. Similarly, CC tumouroids exhibited extensive glandular domains with carcinoma cells forming lumen and growing in cribriform structures, as observed in the original sample (Fig. 1b Suppl. Fig. 2a).
Detailed histological and marker analysis of all the patient's tumour tissues revealed that our cultures derived from a moderate-to-well differentiated HCC (HCC-1, AFP+, HePar1+), a poorly differentiated HCC (HCC-3; AFP+, HepPar1-, EpCAM-), a classical combined (CHC-1; HepPar1+, EpCAM+, mucins +), a combined with stem cell features (CHC-2; AFP+, HepPar1+, EpCAM+) and moderate-to-poorly differentiated CCs (CC-1, -2 and -3; HepPar1-, EpCAM+) (Fig. 2a-b, Suppl. Fig 3a-b and d and Suppl. Table 1) [25]. Subsequent analysis of these subtype-specific markers in the corresponding tumouroids revealed that tumour-derived organoids express the diagnostic markers of their parental tissues, even after long-term expansion in culture in the same culture conditions for the different lines. Thus, EpCAM, marker for CC and CHC tumours [3, 26] was highly expressed in all CCs (CC-1, -2 and -3) and CHCs (CHC-1 and -2) tumouroids and corresponding patients' tissues but absent on HCCs tumouroids and corresponding patients' tissues (Fig. 2c and Suppl. Fig.3b). Likewise, Alpha-fetoprotein (AFP), a well-established marker for HCCs and a subset of CHCs [26], but not expressed in CCs [1, 5, 27, 28], was highly expressed in both HCCs and CHC-2 tumouroids but absent in all CC tumouroids and in the CHC-1 line, in agreement with the expression pattern and diagnostic of the original patient's tissue (Fig. 2c and Suppl Table 1). Remarkably, *SALL4* described for a subset of aggressive HCCs [29, 30] and a subset of CHCs [31] was present only in HCC-3 and CHC-2, both in tumouroids as well as in the corresponding patient's tissue, but absent in all other tissues and tumouroid lines (Suppl. Fig. 3c).

Overall, these results demonstrate that the 3 different subtypes of liver tumour organoids both recapitulated and retained the histological characteristics and marker expression of the original tumour tissue and subtype, even after long-term expansion in culture, in the same culture conditions.

Genome-wide analysis demonstrates that Primary Liver Cancer-derived organoid cultures recapitulate the expression profile of the corresponding tissue-of-origin and tumour subtype.
The gene expression patterns of PLC subtypes (HCC, CC and CHC) have been extensively studied [32] and have proved useful in classifying them [33]. Therefore, to further evaluate

whether tumouroids maintain the expression profile of the original tumour, we opted to characterize in depth these novel PLC-derived organoid lines by comprehensively studying their expression profiles compared to the corresponding parental tissues using genome-wide transcriptomic (RNAseq) analysis. Healthy liver-derived organoid lines growing in expansion and differentiation medium and corresponding healthy liver tissues were used as additional controls.

Strand-specific RNAseq libraries were generated from all organoid lines and corresponding tissue-of-origin (CC-1 to 3; HCC-1 and -3; CHC-1 and -2; Healthy-1 to 3). Relative transcript abundance (transcripts per million, RPKM) of 15,648 gene transcripts was determined. For some samples, several biological as well as technical replicates were run (see Dataset_1_S1 for details). PCA analysis indicated that both, technical and biological replicates per patient were almost identical (data not shown). Hence, to process the data for further analyses we averaged all these technical and biological replicates of each patient tissue or organoid together and present the analysis per patient sample. Gene expression correlation analysis indicated that each tumouroid line correlated to its corresponding tissue-of-origin. Thus, HCC-1 and HCC-3 correlated with HCC-1 and HCC-3 tissues respectively, while all 3 CC tumouroid lines correlated with the corresponding CC but not HCC nor CHC tissues. Similarly, CHC tumouroid significantly correlated to their respective CHC tissues but not to the other subtypes (Fig. 3a). PCA analysis of tissues and corresponding tumouroids revealed that the samples grouped by subtype on the PC2 component, indicating that each PLC-derived organoid subtype is similar to its corresponding tissue subtype, while the PC1 component accounted for the variance between tissues and tumour-derived organoids. Classical HCC markers such as *AFP* or *APOH* and CC markers such as *KRT7* or *MMP7*, were amongst the genes that contribute the most to the variance in the PC2 component (Fig. 3b and Suppl. Dataset 1_S2).

In agreement with the expression of the original tissues, we found the genes *AFP, ALB, APOH, FGG, RBP4*, *TF, AHSG, FGB,* (all involved in HCC progression [34]) and recently described as markers of HCC tumour-circulating cells [35], to be highly upregulated (2Log-FC>6) in HCC tumouroids (Fig. 3c and Suppl. Dataset 1_S2). Also, several markers of differentiated hepatocytes (*TTR, CYP2E1, APOA1, APOE)* were within the most upregulated genes (2LogFC>5) while *TFF2*, a CC marker [36], and the ductal markers *KRT7*, *KRT19, EPCAM* and *CD24* were amongst the most downregulated genes in both HCC tumouroid lines (Fig. 3b-c, Suppl. Fig. 2b, and Suppl. Dataset1 _S2-3). Similarly, in CC tumouroids, *S100P*, *S100A11, S100A6* [37], *ALDOA* [38], *CLIC3 and ANKRD22* [39] all commonly upregulated in CC tissues [40-42] were highly expressed, while hepatocyte (*ALB, TTR, APOA1 and APOE*) and HCC markers (*AFP, GPC3*) [34] were not expressed or strongly downregulated (Fig. 3b-c and Suppl. Dataset 1_S5), in agreement with the expression of the original CC- tumours. *KRT7* and *KRT19* were highly expressed in both CC-derived and healthy liver-derived organoids, as expected due to their ductal/progenitor origin (Fig. 3c, and Suppl. Dataset 1_S5). The CHC lines (CHC-1 and CHC-2) shared the expression of markers of both HCC (*APOA1*, *TTR*, *GPC3*) and CC (*EpCAM, KRT19*) tumours, as expected (Fig. 2c, Fig. 3c, and Suppl. Dataset 1_S4). Remarkably, these markers were also retained in a patient specific manner even within each subtype. For instance, *MUC5B* was expressed only in CHC-1 but not in CHC-2 organoids, in agreement with the corresponding patient's tissues PAS staining (Fig. 3c and Suppl. Fig. 3d), whereas AFP was expressed in CHC-2 but not CHC-1 in concordance with the AFP values in serum of these patients at the moment of resection

(compare Fig. 2c and Suppl. Table 1).

Gene-Set-Enrichment-Analysis (GSEA) of the tumouroid lines and their corresponding parental tissues using 159 published cancer gene-sets (Suppl. Dataset 2_S1 and 3_S1) confirmed that the tumouroid cultures retain the gene expression profile of the specific tumour subtype they derive from, in a patient-specific manner (Fig. 3d and Suppl. Datasets 2-3). Thus, for both HCC lines and corresponding tissues, HCC gene-sets were the most significantly positively enriched, with HCC-1 associated to a gene-set describing HCC with hepatocyte differentiation features while HCC-3 significantly associated with a proliferative HCC subclass and a KRT19 positive subclass gene-sets but showing a negative correlation with the gene-sets related to hepatocyte differentiation and good prognosis, in agreement with the differentiation status of the patient's original tissue (Fig.3d, Suppl. Fig.4 a and c, and Suppl. Dataset 2 and 3). Conversely, for all CC tumouroids and corresponding tissues, CC gene-sets were the most significantly positively enriched whereas HCC specific gene-sets were significantly down-regulated as expected. (Fig.3d, Suppl. Fig.4a and Suppl. Dataset 2 and 3). Similarly, the CHC expression profiles were negatively correlated with HCC-differentiation gene-sets but positively correlated with progenitor/stem cell, proliferation and/or poor prognosis gene-sets (Fig.3d, Suppl. Fig.4 a and Suppl. Dataset 2 and 3).

Subsequent immunofluorescent and qPCR analyses of tumouroids and associated tissues confirmed the RNAseq results indicating that the cultures retained the differentiation status of the parent tumour subtype *in vitro*. Thus, HCC tumouroids exhibited a high degree of hepatocyte differentiation, with high levels of HNF4a and Albumin expression and secretion (Suppl. Fig. 4d-e), with HCC-1 being the most differentiated and exhibiting high production of bile acid in the medium (Suppl. Fig. 4f). Similarly, CHC tumouroids also presented some degree of differentiation, albeit reduced compared to the HCCs, in agreement with their combined phenotype (Suppl. Fig. 4d-e). All of these hepatocyte markers were absent in CC tumouroids (Suppl. Fig 4d). In contrast, KRT19, marker for CC and CHC tumours [3, 26] and a subset of HCCs [25] was highly expressed in all CC (CC-1, CC-2, CC-3), in both CHC (CHC-1 and CHC-2) and in HCC-3 derived tumouroids, but undetectable in the most differentiated HCC-1 line, in agreement with the histological subtype, expression pattern and gene signature of the patient's tumour tissue (Suppl. Fig. 4c-d). Similarly, KRT7, a well-established marker for CCs [43], was only expressed in the CC-derived organoids and corresponding parental tissues, but not in the HCC or CHC tumouroids (Suppl. Fig. 4g).

These results demonstrate that the PLC-derived organoid culture system faithfully recapitulates and maintains the transcriptomic alterations present in the individual patient's tumour subtype. Since the different tumour subtypes were all maintained in the same culture conditions these results suggest that their tumour signature is intrinsic to the cancer population, and is not significantly modified by the culture conditions.

Tumouroid/Organoid cultures allow identification of novel genes involved in liver cancer progression and potentially novel liver cancer biomarkers

We next sought to investigate if the tumouroid culture system, which is enriched on the tumour propagating cells, could represent a valuable resource to identify novel genes involved in PLC progression or novel potential PLC biomarkers, a use not previously described for tumour-derived organoid systems. For that we first defined a tumouroid expression signature by comparing the similarities between the transcriptomes of all

tumouroid lines to healthy liver-derived organoid lines. We defined this gene list as "tumouroid signature" list (Fig. 3e). Notably, within the top 30 most upregulated genes (Suppl. Dataset 1_S6) we found 19 genes already reported to be markers/overexpressed in PLC, 13 of which were already associated to poor-prognosis including *DANCR* [44], *MCM7* [45], *UBE2C* [46] and *CCNB1* [47] (Fig. 3f), thus validating our approach. From the remaining 11 genes, we found 5 genes already associated to other cancers while the remainder had never been associated to cancer.

To determine the value of this tumouroid gene list for diagnostic or prognostic prediction, we performed an in-depth analysis of this top 30 genes by determining their expression pattern and prognostic value in cohorts of primary liver cancer patients and healthy individuals from publically available TCGA databases (for HCC: 374 HCC patients and 50 healthy individuals; for CC: 31 CC patients and 8 healthy individuals). Notably, 29 of the top 30 genes were significantly ($p \leq 0{,}01$) overexpressed in cancer patients *vs* healthy individuals for both cohorts, HCCs and CCs (Fig. 3f and Suppl. Dataset 1_S7), thus exemplifying the value of PLC-derived organoids to identify genes involved in primary liver cancer. Of note, 18 of these genes also exhibited significant predictive prognostic value, i.e., predicted poor prognosis when overexpressed. Importantly, from these genes we found 5 novel genes associated to poor survival in the different PLC cancer cohorts: *C19ORF48, UBE2S* and *DTYMK* (for HCC) and *C1QBP* and *STMN1* (for CC). Of note, none of these genes had been previously associated to liver cancer, except for *STMN1,* that had been associated to poor prognosis in HCC but not in CC [48] (Fig 3f-h). Therefore, these results demonstrate that growing primary liver cancer as tumouroids preserves the tumour-cell features at a level that allows identifying potential new genes involved in PLC progression. In addition, these genes could potentially be used as prognostic markers in primary liver cancer.

Overall these results highlight two important advantages of the tumour-derived organoid culture system: (1) the ability to faithfully recapitulate and maintain the transcriptomic alterations present in the individual patient's tumour subtype and (2) its potential for liver cancer biomarker discovery.

Liver tumouroids retain the genetic alterations present in the original tumour tissue.
PLCs, in particular CC, HCC and CHC, typically present with a high degree of aneuploidy and share several copy number changes, somatic mutations and epigenetic alterations [6]. All the tumouroid lines that we expanded in culture (HCC, n=2; CHC, n=2; CC, n=3) exhibited multiple chromosomal aberrations consisting of both gains and/or losses of chromosome numbers (Fig. 4a-b). This was in stark contrast to healthy liver-derived organoids that stably maintained diploid chromosome numbers in culture, in agreement with our previous observations [23] [49]. To determine whether the different tumouroid lines retain the parent tumour's mutational landscape, we performed whole exome sequencing (WES) analysis of each liver tumouroid line expanded for short (<2 months, early passage) or extended (>4 months, late passage) periods in culture and compared the results to the corresponding parent tumour.

We generated ~19 Gb exome DNA sequence data from each sample. After removal of low quality reads (<Q20) and adaptor sequences, we identified and selected the variants with the following parameters: base quality ≥15 (Phred score), read depth ≥15 and annotated as not

"intergenic" (see methods for details). When comparing the mutational burden in the patient's tissue to its corresponding tumouroid lines, we observed a strong correlation between the somatic variations of each tumouroid and corresponding original tissue (Fig. 4c). We found that an average of ~92% of the somatic variants in the patient's tissue were retained in the corresponding early tumouroid cultures (<2months), and >80% even after months of expansion (Fig. 4c). Similarly, the analysis of the number of mutations for both patient's tissue and corresponding tumouroid cultures confirmed that the global SNV number as well as the number of indels in the original patient tissue is well retained in culture, even at late passage (Fig. 4f). The distribution of somatic base substitutions for both tissues and organoids revealed an over-representation of the nucleotide transversion T>C/A>G and C>T/G>A, in agreement with the mutational spectrum described for CCs and HCCs [50, 51] (Fig 4d-e). Of note, we did not find significant bias between transcribed and untranscribed strands (Suppl Fig. 5a). After applying an additional filtering step aimed at identifying cancer related variants (filtering SNVs present in COSMIC databases but excluding dbSNPs) we also found that the majority of all the cancer-related somatic variants present in the patient's original tissue (>75%) were retained in the corresponding tumouroid cultures in both early and late passage. In fact, <10% of these cancer-related variants were lost between tissue and early organoids, thus suggesting that the cultures represent the tumour genetic landscape of the original patient with little bias for sub-populations of tumoral cells harbouring specific mutations (Fig. 4f).

The detailed analysis of the specific somatic mutations present in both tissues and corresponding organoids, showed that all lines harboured the TP53 missense variant P72R, with CHC-2 also presenting 1 additional frameshift variants (L206fs) (Fig. 4g and Suppl. Dataset 4). In addition, HCC-1 and HCC-3 lines exhibited missense mutations in *CTNNB1*, while the Wnt negative regulator *RNF43* was found mutated only in CC-derived tumouroids (Fig. 4g and Suppl. Dataset 4) in agreement with the differential mutational pattern of these 2 components of the Wnt pathway in these 2 subtypes of liver tumours [52, 53, 54]. Consequently, these results correlated with the significant enrichment in *β-catenin* mutated liver cancer datasets for HCC-1 (Fig. 3d) and the ability of HCC but not CC lines to grow and express the Wnt target genes *TNFSRF19, AXIN2* and *LGR5* in the presence of the porcupine inhibitor IWP2 in the medium (Suppl. Fig. 5d-e). Similarly, we also identified mutations in *KRAS* (*KRASG12D*) in CC-1 and CHC-1 tumouroids but not in the other lines, in agreement with the transcriptomic analysis, which showed significant enrichment in published EGF activated dataset (Suppl. Fig. 5c) [55]. Notably, we found nonsense mutations (frameshifts or stop-gains) in the chromatin remodelling genes *ARID1A* (HCC-3 and CC-1), *ARID2* (HCC-3) and *BAP1* (CHC-1), in agreement with previous reports that have highlighted the importance of these genes in both types of primary liver cancers [56, 57] (Fig.4g, and Suppl. Dataset 4). All lines were devoid of mutations in *MAPK1* and *MAPK3* (ERK1 and ERK2 respectively) (Fig. 4g), in agreement with previous studies in primary liver cancer [58].

Therefore, these results indicate that the PLC tumouroid culture system retained the mutational landscape of the original tumour tissue and faithfully retained the tumour-specific mutations present in the original sample from which where derived.

Tumouroids recapitulate parent tumour histology and metastatic potential *in vivo*

To determine whether tumouroids also recapitulate the features of a human primary liver tumour *in vivo*, we transplanted CC (CC-1, -2 and -3 lines) and HCC-1 long-term expanded tumouroids under the skin of immunocompromised mice (Fig. 5 and Suppl. Fig. 6). Healthy liver-derived organoids were used as controls. We found tumour outgrowths in the animals engrafted with CC-1_O (29/29), CC-2_O (8/8) and HCC-1_O (24/34) (Fig. 5b and Suppl. Fig. 6a-b). As expected, healthy liver-derived organoids (Healthy-1_O) did not generate any tumoural mass in any of the animals engrafted (Fig. 5b and Suppl. Fig. 6b). The CC- derived tumours exhibited a strong stromal reaction and a histological pattern that closely resembled the architecture of the patient's tumour tissue. Thus, CC-1_O tumours presented with proliferative KRT19+ cells forming glands with cribriform structures (Fig. 5d), while CC-2_O tumours exhibited a more differentiated phenotype, reminiscent of the CC-2-patient original tissue (Suppl. Fig.6d). Similarly, HCC-1_O derived tumours grew as a solid mass that recapitulated the histological architecture of the original HCC tumour with pseudoglandular rosettes present also in the grafted tissue (Fig.5e). Of note, secondary tumouroids could be derived from the xenografted tumours. These exhibited similar chromosome counts and were morphologically and histologically indistinguishable from their parental tumouroid line (Suppl. Fig.6g-h), thus indicating that even after long-term expansion *in vitro* and transplantation *in vivo*, expanding primary liver tumours of both HCC or CC subtypes in organoid culture methods, stably preserves the histological architecture of the parent tumour.

Liver cancer has been reported to metastasize primarily to the lung and portal lymph nodes [59]. To determine whether our tumouroid models would faithfully recapitulate liver cancer metastatic phenotype, we injected a line derived from a patient with history of metastasis (CC-1_O) into the kidney capsule of NSG mice (Fig.5c). As expected, 100% of the injected mice developed tumours that resembled the original patient tissue (Fig.5f). More importantly, in 7 out of 9 of the injected mice we also found secondary metastases in the lung (Fig.5c and g and Suppl. Fig.6f), in agreement with the patient's diagnostic at the moment of resection, where metastatic nodules had been detected (Suppl. Table 1). Healthy liver-derived organoids (Healthy-1_O) did not generate any metastases, as expected (Fig. 5c and g and Suppl. Fig.6f).

Overall, these results establish that primary liver cancer-derived organoids accurately model the histological and metastatic features of their parent tumours *in vivo,* even after long-term expansion in culture.

Liver tumouroids allow the identification of patient-specific drug sensitivities and highlight ERK as a potential target for liver cancer

We performed proof-of-concept drug sensitivity testing in 6 of the PLC tumouroids lines (HCC-1, HCC-3, CHC-1, CHC-2, CC-1 and CC-2) to evaluate their use to identify patient-specific sensitivities and as a platform to inform drug development. As an initial prioritization step, for each tumouroid line we tested their sensitivity to 29 anti-cancer compounds targeting key proteins and pathways implicated in cancer, including several drugs in clinical use or development. Tumouroids were plated on BME-coated 384-well plates and treated with a 7-point, half-log dilution series of each compound for 6 days, before measuring cell viability [60]. Drug sensitivity was represented by the area under the dose response curve (AUC) (Fig. 6a and c, Suppl. Dataset 5) and by the half-maximal inhibitory concentration (IC_{50}) (Fig. 6c and Suppl. Dataset 5). The assay was conducted with technical replicates and two biological replicates per tumouroid were independently screened.

There was a positive correlation of biological AUC replicates (R_p = 0.79) and IC_{50} replicates (R_p = 0.73) across the dataset. Observed variation was in part due to the large size of tumouroids leading to uneven distribution in screening wells. CC-2 was insensitive to all compounds in the screen and so was excluded from further analyses. Overall, tumouroids were resistant to the majority of the compounds, with an IC_{50} greater than the maximum screening concentration, although we detected interesting sensitivity to several compounds (Fig.6a-c). For instance, we found all lines were resistant to the MDM2 inhibitor nutlin-3a, in agreement with all of them harbouring *TP53* mutations. Similarly, HCC-1 and HCC-3, harbouring mutations in *b-catenin*, were resistant to the porcupine inhibitor LGK974, whereas CC-1 was sensitive (Fig 6a-c), in concordance with our previous results with another porcupine inhibitor, IWP2 (Suppl. Fig 5d-e). We observed tumouroid sensitivity to Gemcitabine, which is used clinically for the treatment of PLC patients (Fig 6a-c).

From our initial prioritization screen, we confirmed drug sensitivity for a subset of compounds using a tumouroid formation assay. We selected clinically relevant compounds where differential sensitivity was observed across the tumouroid panel; namely Taselisib, Gemcitabine, AZD8931, SCH772984 and Dasatanib (Fig. 6c-d). Overall, a good agreement between the screening and validation results was observed (suppl.Figure 7a). An exception was for CC-1 line with AZD8931, where we observed a variable sensitivity between biological replicates in the prioritization screen. The validation screen confirmed that PI3Kα inhibition with the preclinical compound Taselisib (10μM) resulted in a growth inhibitory effect in 5 of 6 tumouroids, in line with all these tumouroids being WT for PIK3CA and RSK2 (*RPS6KA3*). EGFR-family inhibition with 5μM AZD8931 restricted tumouroid formation in HCC-1 cells, whereas the other lines were resistant. Sensitivity to EGFR inhibition in HCC-1 cells was confirmed with a second EGFR inhibitor Gefitinib, which was not present in our screen (Suppl.Fig.7b). Similarly, Dasatinib (2μM) suppressed tumouroid formation in CC-1 cells, in agreement with our screening results (Fig.6 c-d).

Of particular interest was the substantial inhibition of tumouroid formation following inhibition of ERK1/2 by SCH772984 in both HCC lines, as well as in the other tumouroid subtypes, CC-1 and CHC-1 cells (Fig. 6a-d and Suppl. Fig.7a). SCH772984, which selectively inhibited ERK-phosphorylation in HCC-1 and CC-1 tumouroids (Suppl. Fig.7f), was effective in lines that were insensitive to the BRAF and/or MEK inhibitors in our screen (Dabrafenib and Trametinib) (Fig.6c). The reason for this difference is unclear, although ERK inhibitors have demonstrated activity in cells with acquired BRAF and MEK inhibitor-resistance [61].

We note that clinical trials exploring the effect of specific ERK inhibitors for PLC have not been reported thus far. Hence, to further investigate the potential of ERK1/2 inhibition for PLC, we tested the efficacy of SCH772984 to inhibit tumour growth *in vivo*. For that, CC-1 and HCC-1-derived tumouroids were transplanted subcutaneously into NSG mice and, when tumours reached a mean volume of ~100mm^3, we injected them intra-tumourally with either SCH772984 or with the vehicle for a 10 to 15 day period. Remarkably, 2-7 days after the first injection we observed a significant reduction in tumour growth, which lasted for the remainder of the experiment up to 24 days (Fig.6e and Suppl. Fig. 7d). Histological analysis of the tumours from both CC-1 and HCC-1 lines at 24-25 days after treatment initiation, when a significant tumour regression was observed, revealed that the tumour mass was necrotic and that the majority of the cells were apoptotic (Fig.6f-g and Suppl. Fig. 7e). Western blot analysis from tumours treated for 6 hours with either SCH772984, or with the vehicle control,

confirmed that SCH772984 also *in vivo* selectively inhibited ERK-phosphorylation in CC-1 tumours (Suppl. Fig. 7g). Thus, in aggregate, our proof-of-concept study demonstrates the application of PLC tumouroids for *in vitro* and *in vivo* drug testing, and provides initial evidence that ERK inhibition could have a beneficial therapeutic effect on a subset of HCC and CC patients.

Overall, these results indicate that by faithfully retaining the histological, transcriptomic and genomic landscape of their parent tumour, tumouroid cultures facilitate the prediction of drug sensitivity/resistance in a patient-specific manner. They therefore, provide an important new resource for liver cancer research, opening up new avenues for biomarker discovery and drug testing as well as to gain further insights of the origin and progression of an increasingly prevalent disease.

DISCUSSION

The advent of 3D culture systems has made it possible to partially recapitulate the complexity and function of mammalian tissue *in vitro*, by forming structures that resemble an adult organ in culture and which have been termed "organoids" [15]. Based on the knowledge from small intestine, we recently have demonstrated that gastric, pancreatic and hepatic organoid cultures derived from either adult mouse or human tissues self-renew and differentiate *in vitro*, into the corresponding cell types of the tissue-of–origin [14, 15].

Here, we demonstrate the proof-of-concept that primary liver cancer (PLC) tissue grown as organoid cultures (here termed tumouroid) faithfully models the genetic complexity of human PLC *in vitro*. We successfully established cultures from tumours derived from 8 PLC patients representing the three most common subtypes of PLC [1]: HCC, CC and CHC. In contrast to any liver cancer cell line grown in 2D, PLC-derived organoids recapitulate the histological architecture and expression profiles of the corresponding parent tumour, even after being cultured long-term in the same culture conditions for all subtypes or upon transplantation into mice. Notably, they also retain the specific differences between patients as well as between tumour subtypes. We have exploited this aspect here to demonstrate that tumour-derived organoid cultures represent a valuable resource for biomarker discovery, especially for prognostic markers, an application not previously reported for any organoid culture system. In fact, tumour organoids encompass cells with long-term self-renewal capacity but are devoid of any stromal component. This represents an advantage for gene discovery, as it facilitates enrichment of the tumour propagating population, thus facilitating the identification of relevant genes involved in liver cancer and potential new biomarkers. Here we report *C19ORF48, UBE2S, DTYMK, C1QBP* and *STMN1* as all novel predictors of poor prognosis for primary liver cancer. These results open up novel opportunities in using tumour-derived organoids for tumour marker discovery.

A unique and important feature of the tumouroids is that they maintain the mutational landscape of the original patient's tumour, even after long-term expansion in culture or following transplantation and derivation into secondary organoids. This is vastly different to existing 2D cell lines, which albeit they cover the major driver mutations observed in many cancer sub-types [62], no longer present the patient-specific signature and genetic landscape of the original tumours from whence they were derived, exemplified by the frequent acquisition of mutations in p53 in such cell lines [63]. The reasons for these differences are unknown, but it is feasible to speculate that the cell-matrix interactions may play an important role. In fact, embedding primary tumoural epithelial cells within an extracellular matrix (ECM) enables the cells to interpret the environment and self-assemble into structures which acquire tissue patterning, as it occurs during development and organogenesis. Also, the cell-matrix interactions established in 3D could prevent anoikis-apoptosis due to detachment from the matrix[64] of those tumoural cells that have not acquired yet all the mutations to survive in a ECM-free milieu, thus facilitating the maintenance of heterogeneous, non-selected populations within the culture. In that line, our results indicate that if selection of specific tumoural cells exist in the cultures, this might have a minor effect at the population level, as we found that tumouroids harbour >92% of the mutations present in the original tissue.

The reproduction of parent tumour genetic aberrations in a culture setting makes tumouroid lines a potentially valuable resource in screening drug sensitivity/resistance, identifying novel

players in liver cancer progression, or even novel therapeutics as part of a personalized medicine approach. Our results validate such an approach by (1) demonstrating a correlation between drug sensitivity and mutational profile in the tumouroid lines and (2) the *de novo* identification of the ERK inhibitor SCH772984 as a potential novel therapeutic agent for liver cancer.

The lack of immune system and stromal components, though, represents a limitation of the culture system, especially when aiming at studying tumour cell-stroma/immune interactions. In that regard, patient derived xenografts (PDXs) have proven useful models for human cancer, including liver cancer [13, 65], as they also retain tumour histopathology, including tumour-infiltrating lymphocytes and the stromal component, and global gene expression and methylation profiles of the patient's malignant epithelial cells [66]. However, PDXs suffer from a low engraftment rate, especially CCs (5.8% engraftment efficiency as reported by [13]), have a long engraftment period (often several months), they are expensive and time-consuming, and are not tractable for large-scale drug sensitivity testing [66]. Therefore, we believe that the PLC-derived organoid cultures we present here are complementary and alternative models to liver cancer PDXs. Specifically, the derivation efficiency is ~75%, especially for CC, and is significantly shorter than for PDX. Furthermore, they are suitable for large-scale drug testing, and in a timescale that makes potentially compatible with personalized medicine approaches.

In conclusion, the PLC-derived organoids that we present here fulfil all the criteria of a reliable *in vitro* cancer model, recapitulating all the features of three of the most common subtypes of liver tumours, from histological architecture to genetic and transcriptomic traits, and are amenable as a platform for drug testing. With a short timescale from establishment to drug testing, this novel *in vitro* liver cancer system thus makes hitherto inaccessible possibilities for predicting patient-specific drug responses and creating personalized/*à la carte* therapies into a reality.

ACKNOWLEDGEMENTS

M.H. is a Wellcome Trust Sir Henry Dale Fellow and is jointly funded by the Wellcome Trust and the Royal Society (104151/Z/14/Z). L.B. is supported by an EMBO Postdoctoral fellowship (EMBO ALTF 794-2014) and Marie-Curie Postdoctoral fellowship (Grant 656193_H2020-MSCA-IF-2014). G.M. is supported by a Marie Curie Initial Training Network (WntsApp). This work was supported by a NC3Rs International prize, a Beit Prize and a Cambridge Cancer Center-pump priming award all of them awarded to M.H. Work at the L.J.W.v.d.L lab was funded by the research program InnoSysTox, [project number 114027003], by the Netherlands Organisation for Health Research and Development (ZonMw) and part of the research program financed by the Dutch Digestive Foundation [MLDS-Diagnostics project number D16-26]. Work in the MJG lab is funded by the Wellcome Trust (102696), Stand Up To Cancer (SU2C-AACRDT1213), and Cancer Research UK (C44943/A22536).
M.H. would like to thank Prof Brigid Hogan (Chapel Hill) and Prof Magdalena Zernicka-Goetz (University of Cambridge) for helpful discussions and critical comments. We also thank Dr Chris Hindley for editorial assistance, The Gurdon Institute facilities for assistance with imaging and animal care. Dr. Sylviane Moss and Dr Maike Paramor for technical assistance with sequencing analysis and Dr Asif Jah (Cambridge University Hospitals NHS Trust) for facilitating recruitment of patients.

AUTHOR CONTRIBUTIONS

L.B., designed and performed experiments and interpreted results. G.M., and M.H., performed experiments and interpreted results. R.A., performed experiments. L.M.G., C.R.B., G.E.A. and S.D. performed bioinformatic analyses. S.E.D., performed the histopathology diagnosis. M.M.A.V., M.P.G, R.L., J.N.M.I.J., S.J.W, R.K.P., N.G. and K.S.P., provided patient material and interpreted clinical data. K.S.P., performed the kidney capsule transplants. H.E.F. and M.J.G. performed the drug screening, interpreted the results and wrote this section of the manuscript. M.H. conceived and designed the project. L.B. and M.H. wrote the manuscript. All authors commented on the manuscript.

COMPETING FINANCIAL INTERESTS

The authors declare no competing financial interests.

REFERENCES

1. Hirohashi, S., et al., *Tumours of the Liver and Intrahepatic Bile Ducts*, in *World Health Organization Classification of Tumours*, M.D. Stanley R. Hamilton and M.D. Lauri A. Aaltonen, Ph.D., Editors. 2000, IARCPress: 69372 Lyon, France.
2. Bosch, F.X., et al., *Primary liver cancer: Worldwide incidence and trends.* Gastroenterology, 2004. **127**(5, Supplement 1): p. S5-S16.
3. Bridgewater, J., et al., *Guidelines for the diagnosis and management of intrahepatic cholangiocarcinoma.* Journal of Hepatology, 2014. **60**(6): p. 1268-1289.
4. Lee, S.D., et al., *Clinicopathological features and prognosis of combined hepatocellular carcinoma and cholangiocarcinoma after surgery.* Hepatobiliary Pancreat Dis Int, 2014. **13**(6): p. 594-601.
5. International Consensus Group for Hepatocellular, N., *Pathologic diagnosis of early hepatocellular carcinoma: A report of the international consensus group for hepatocellular neoplasia.* Hepatology, 2009. **49**(2): p. 658-664.
6. Marquardt, J.U. and J.B. Andersen, *Liver cancer oncogenomics: opportunities and dilemmas for clinical applications.* Hepatic oncology, 2015. **2**(1): p. 79-93.
7. Wang, A.-Q., et al., *Combined hepatocellular cholangiocarcinoma: Controversies to be addressed.* World Journal of Gastroenterology, 2016. **22**(18): p. 4459-4465.
8. Sharma, S.V., D.A. Haber, and J. Settleman, *Cell line-based platforms to evaluate the therapeutic efficacy of candidate anticancer agents.* Nat Rev Cancer, 2010. **10**(4): p. 241-53.
9. De Minicis, S., et al., *Liver carcinogenesis: Rodent models of hepatocarcinoma and cholangiocarcinoma.* Digestive and Liver Disease, 2013. **45**(6): p. 450-459.
10. Oikawa, T., et al., *Model of fibrolamellar hepatocellular carcinomas reveals striking enrichment in cancer stem cells.* Nature Communications, 2015. **6**: p. 8070.
11. Shamir, E.R. and A.J. Ewald, *Three-dimensional organotypic culture: experimental models of mammalian biology and disease.* Nature reviews Molecular cell biology, 2014. **15**(10): p. 647-664.
12. Ku, J.L., et al., *Establishment and characterisation of six human biliary tract cancer cell lines.* British Journal of Cancer, 2002. **87**(2): p. 187-193.
13. Cavalloni, G., et al., *Establishment and characterization of a human intrahepatic cholangiocarcinoma cell line derived from an Italian patient.* Tumour Biology, 2016. **37**(3): p. 4041-4052.
14. Hindley, C.J., L. Cordero-Espinoza, and M. Huch, *Organoids from adult liver and pancreas: Stem cell biology and biomedical utility.* Developmental Biology.

15. Huch, M. and B.-K. Koo, *Modeling mouse and human development using organoid cultures.* Development, 2015. **142**(18): p. 3113-3125.
16. Li, X., et al., *Oncogenic transformation of diverse gastrointestinal tissues in primary organoid culture.* Nature medicine, 2014. **20**(7): p. 769-777.
17. Sato, T., et al., *Long-term Expansion of Epithelial Organoids From Human Colon, Adenoma, Adenocarcinoma, and Barrett's Epithelium.* Gastroenterology, 2011. **141**(5): p. 1762-1772.
18. van de Wetering, M., et al., *Prospective derivation of a living organoid biobank of colorectal cancer patients.* Cell, 2015. **161**(4): p. 933-45.
19. Boj, S.F., et al., *Organoid Models of Human and Mouse Ductal Pancreatic Cancer.* Cell, 2015. **160**(0): p. 324-338.
20. Gao, D., et al., *Organoid Cultures Derived from Patients with Advanced Prostate Cancer.* Cell, 2014. **159**(1): p. 176-187.
21. Huch, M., et al., *Unlimited in vitro expansion of adult bi-potent pancreas progenitors through the Lgr5/R-spondin axis.* The EMBO Journal, 2013. **32**(20): p. 2708-2721.
22. Huch, M., et al., *In vitro expansion of single Lgr5+ liver stem cells induced by Wnt-driven regeneration.* Nature, 2013. **494**(7436): p. 247-250.
23. Huch, M., et al., *Long-Term Culture of Genome-Stable Bipotent Stem Cells from Adult Human Liver.* Cell, 2015. **160**(1–2): p. 299-312.
24. Broutier, L., et al., *Culture and establishment of self-renewing human and mouse adult liver and pancreas 3D organoids and their genetic manipulation.* Nat Protoc, 2016. **11**(9): p. 1724-43.
25. Brunt, E.M.P., V.; Sempoux, C.; Theise, N.D., *Biphenotypic (hepatobiliary) primary liver carcinomas: the work in progress.* Hepatic Oncology, 2015. **2**: p. 18.
26. Zhang, F., et al., *Combined hepatocellular cholangiocarcinoma originating from hepatic progenitor cells: immunohistochemical and double-fluorescence immunostaining evidence.* Histopathology, 2008. **52**(2): p. 224-232.
27. Zhao, Y.-J., Q. Ju, and G.-C. Li, *Tumor markers for hepatocellular carcinoma.* Molecular and Clinical Oncology, 2013. **1**(4): p. 593-598.
28. Ohguchi, S., et al., *Expression of α-fetoprotein and albumin genes in human hepatocellular carcinomas: Limitations in the application of the genes for targeting human hepatocellular carcinoma in gene therapy.* Hepatology, 1998. **27**(2): p. 599-607.
29. Yakaboski, E., A. Jares, and Y. Ma, *Stem cell gene SALL4 in aggressive hepatocellular carcinoma: a cancer stem cell-specific target?* Hepatology, 2014. **60**(1): p. 419-21.
30. Yong, K.J., et al., *Oncofetal gene SALL4 in aggressive hepatocellular carcinoma.* N Engl J Med, 2013. **368**(24): p. 2266-76.
31. Moeini, A., et al., *Mixed hepatocellular cholangiocarcinoma tumors: Cholangiolocellular carcinoma is a distinct molecular entity.* J Hepatol, 2017. **66**(5): p. 952-961.

32. Shibata, T. and H. Aburatani, *Exploration of liver cancer genomes.* Nature Reviews Gastroenterology & Hepatology, 2014. **11**: p. 340-349.
33. Woo, H.G., et al., *Identification of a cholangiocarcinoma-like gene expression trait in hepatocellular carcinoma.* Cancer research, 2010. **70**(8): p. 3034-3041.
34. Wang, L., et al., *AFP computational secreted network construction and analysis between human hepatocellular carcinoma (HCC) and no-tumor hepatitis/cirrhotic liver tissues.* Tumor Biology, 2010. **31**(5): p. 417-425.
35. Kalinich, M., et al., *An RNA-based signature enables high specificity detection of circulating tumor cells in hepatocellular carcinoma.* Proc Natl Acad Sci U S A, 2017. **114**(5): p. 1123-1128.
36. Kamlua, S., et al., *A novel TFF2 splice variant (ΔEX2TFF2) correlates with longer overall survival time in cholangiocarcinoma.* Oncology Reports, 2012. **27**(4): p. 1207-1212.
37. Kraiklang, R., et al., *A novel predictive equation for potential diagnosis of cholangiocarcinoma.* PLoS One, 2014. **9**(2): p. e89337.
38. Dos Santos, A., et al., *Identification of cellular targets in human intrahepatic cholangiocarcinoma using laser microdissection and accurate mass and time tag proteomics.* Mol Cell Proteomics, 2010. **9**(9): p. 1991-2004.
39. Andersen, J.B., et al., *Genomic and genetic characterization of cholangiocarcinoma identifies therapeutic targets for tyrosine kinase inhibitors.* Gastroenterology, 2012. **142**(4): p. 1021-1031 e15.
40. Andersen, J.B. and S.S. Thorgeirsson, *Genetic profiling of intrahepatic cholangiocarcinoma.* Curr Opin Gastroenterol, 2012. **28**(3): p. 266-72.
41. Lodi, C., et al., *Claudin-4 differentiates biliary tract cancers from hepatocellular carcinomas.* Mod Pathol, 2006. **19**(3): p. 460-9.
42. Nakajima, T., et al., *Reversal of multiple drug resistance in cholangiocarcinoma by the glutathione S-transferase-pi-specific inhibitor O1-hexadecyl-gamma-glutamyl-S-benzylcysteinyl-D-phenylglycine ethylester.* J Pharmacol Exp Ther, 2003. **306**(3): p. 861-9.
43. Banales, J.M., et al., *Expert consensus document: Cholangiocarcinoma: current knowledge and future perspectives consensus statement from the European Network for the Study of Cholangiocarcinoma (ENS-CCA).* Nat Rev Gastroenterol Hepatol, 2016. **13**(5): p. 261-80.
44. Yuan, S.X., et al., *Long noncoding RNA DANCR increases stemness features of hepatocellular carcinoma by derepression of CTNNB1.* Hepatology, 2016. **63**(2): p. 499-511.
45. Qu, K., et al., *MCM7 promotes cancer progression through cyclin D1-dependent signaling and serves as a prognostic marker for patients with hepatocellular carcinoma.* Cell Death Dis, 2017. **8**(2): p. e2603.
46. Ieta, K., et al., *Identification of overexpressed genes in hepatocellular carcinoma, with special reference to ubiquitin-conjugating enzyme E2C gene expression.* Int J Cancer, 2007. **121**(1): p. 33-8.

47. Weng, L., et al., *Identification of cyclin B1 and Sec62 as biomarkers for recurrence in patients with HBV-related hepatocellular carcinoma after surgical resection.* Mol Cancer, 2012. **11**: p. 39.
48. Hsieh, S.Y., et al., *Stathmin1 overexpression associated with polyploidy, tumor-cell invasion, early recurrence, and poor prognosis in human hepatoma.* Mol Carcinog, 2010. **49**(5): p. 476-87.
49. Blokzijl, F., et al., *Tissue-specific mutation accumulation in human adult stem cells during life.* Nature, 2016. **538**(7624): p. 260-264.
50. Zou, S., et al., *Mutational landscape of intrahepatic cholangiocarcinoma.* Nat Commun, 2014. **5**: p. 5696.
51. Totoki, Y., et al., *High-resolution characterization of a hepatocellular carcinoma genome.* Nat Genet, 2011. **43**(5): p. 464-9.
52. Boulter, L., et al., *WNT signaling drives cholangiocarcinoma growth and can be pharmacologically inhibited.* J Clin Invest, 2015. **125**(3): p. 1269-85.
53. Guichard, C., et al., *Integrated analysis of somatic mutations and focal copy-number changes identifies key genes and pathways in hepatocellular carcinoma.* Nat Genet, 2012. **44**(6): p. 694-8.
54. Ong, C.K., et al., *Exome sequencing of liver fluke-associated cholangiocarcinoma.* Nat Genet, 2012. **44**(6): p. 690-3.
55. Borlak, J., et al., *Epidermal growth factor-induced hepatocellular carcinoma: gene expression profiles in precursor lesions, early stage and solitary tumours.* Oncogene, 2005. **24**(11): p. 1809-19.
56. Jiao, Y., et al., *Exome sequencing identifies frequent inactivating mutations in BAP1, ARID1A and PBRM1 in intrahepatic cholangiocarcinomas.* Nat Genet, 2013. **45**(12): p. 1470-3.
57. Li, M., et al., *Inactivating mutations of the chromatin remodeling gene ARID2 in hepatocellular carcinoma.* Nat Genet, 2011. **43**(9): p. 828-9.
58. Schulze, K., et al., *Exome sequencing of hepatocellular carcinomas identifies new mutational signatures and potential therapeutic targets.* Nat Genet, 2015. **47**(5): p. 505-11.
59. Lee, Y.T. and D.A. Geer, *Primary liver cancer: pattern of metastasis.* J Surg Oncol, 1987. **36**(1): p. 26-31.
60. Francies, H.E., et al., *Drug Sensitivity Assays of Human Cancer Organoid Cultures.* Methods Mol Biol, 2016.
61. Morris, E.J., et al., *Discovery of a novel ERK inhibitor with activity in models of acquired resistance to BRAF and MEK inhibitors.* Cancer Discov, 2013. **3**(7): p. 742-50.
62. Iorio, F., et al., *A Landscape of Pharmacogenomic Interactions in Cancer.* Cell, 2016. **166**(3): p. 740-54.
63. Drexler, H.G., et al., *p53 alterations in human leukemia-lymphoma cell lines: in vitroartifact or prerequisite for cell immortalization?* Leukemia, 2000. **14**(1): p. 198-206.

64. Frisch, S.M., M. Schaller, and B. Cieply, *Mechanisms that link the oncogenic epithelial–mesenchymal transition to suppression of anoikis.* Journal of Cell Science, 2013. **126**(1): p. 21-29.
65. Gu, Q., et al., *Genomic characterization of a large panel of patient-derived hepatocellular carcinoma xenograft tumor models for preclinical development.* Oncotarget, 2015. **6**(24): p. 20160-76.
66. Hidalgo, M., et al., *Patient-derived xenograft models: an emerging platform for translational cancer research.* Cancer Discov, 2014. **4**(9): p. 998-1013.

FIGURE LEGENDS

Figure 1: Patient-derived primary liver cancer organoid cultures expand long-term *in vitro* while preserving the histological architecture of the specific subtype of primary liver tumour they derived from.

(a) Experimental design. For each tissue, samples were split into 4 parts and processed for histology, RNA and DNA isolation, or dissociated and processed for organoid culture. Healthy (donor-derived) liver tissues, moderate/well differentiated hepatocellular carcinoma (HCC), combined hepatocellular-cholangiocarcinoma (CHC) and cholangiocarcinoma samples (CC) were obtained from patients undergoing surgery (patient's information detailed in Supplementary Table 1) and were processed as described in Methods and Suppl. Fig.1. **(b)** Representative H&E staining of healthy liver tissue and primary tumour (top row), and corresponding brightfield microscopy images (middle row) and H&E histological analysis of the organoid lines derived from these (bottom row). Note that, while healthy liver-derived organoids (left) grew as single layered epithelium of ductal-like cells surrounding a central lumen (*, duct; L, lumen), tumour-derived organoids (= tumouroids) formed solid/compacted structures that resembled the corresponding tumour-of-origin [compare tissue (top row) with the corresponding organoid histology (bottom row)]. HCC-1 tumouroids exhibit pseudoglandular rosettes (arrowheads, bottom row), a hallmark of HCC, also found in the parent tumour tissue (arrowheads, top row). CC-1 tumouroids, present a glandular lumen, similar to the original patient's tumour (top row). Scale bars, middle rows 100µm; top and bottom rows, 50µm. Brightfield and H&E pictures from other lines are provided in Suppl. Fig. 2. **(c)** Organoid formation efficiency in classical human healthy liver isolation medium (see Broutier et al, 2016 for details) and tumouroid specific isolation medium (classical human healthy liver complete medium without RSPO + 3nM Dexamethasone - see Methods and Suppl. Fig1 for details). Graph represents mean±SD of the total number of tumouroids obtained per well of each condition. **(d)** Expansion potential of tumouroid cultures established and their correlation to the expansion of healthy-tissue derived organoids. Arrow, continuous expansion. Dot, passage.

Figure 2: Immunohistochemistry analyses reveal that the PLC tumouroids retain expression patterns of the distinct subtype of the original tissue they derived from, even after long-term expansion in culture.

(a) Schematic representation of the multiple subtypes among types of primary liver cancers (PLC). **(b)** IHC assays on the PLC tissues including hepatocyte/HCC marker (HepPar1) and ductal/CC marker (KRT19). Scale bar, 125 µm. Dashed red square indicates focal staining. **(c)** Immunofluorescent analysis for the HCC marker AFP (in red) and the ductal/CC marker EpCAM (in green), on tumouroids expanded in culture for at least 3 months. Nuclei were counterstained with Hoechst33342. Scale bar, 30µm.

Figure 3: Genome wide gene expression analysis indicates that the tumouroids recapitulate the expression profile of the specific subtype of primary liver cancer (PLC) they were derived from and allow identifying potential new genes involved in PLC.

(a) Correlation heat map between PLC-tissue (_T) and paired PLC-derived organoid line (_O) expression profiles showing that the tumourigenic profile of the original tissue and specific subtype of PLC is maintained after long-term expansion in culture. Red, strong correlation; blue, low correlation. **(b)** PCA analysis showing samples plotted in 2 dimensions using their projections onto the first two principal components (PC1 and PC2). Each data point represents one sample, dot stands for tumouroids lines, triangle for PLC tissues. PC1 is

strongly correlated with the type of sample (tumouroids vs tissue) whereas PC2 defines the 3 different PLC subtypes (HCC, CHC and CC). Of note, tumouroid lines and tissues are distributed consistently along PC2 according to their own PLC subtype. Some genes from the top 100 genes with highest loadings across PC2 are shown. **(c)** Heat map analysis of the log2 RPKM values (raw z-scored) of selected genes found highly expressed (red) in HCC and/or CHC and/or CC tumouroids. **(d)** Gene set enrichement analysis (GSEA) comparing the tumouroid lines' and associated tissues' gene expression signatures to 159 curated gene-sets associated with liver cancer and stem cell (representative plots shown in Suppl. Fig. 4). The heatmap shows some of the significantly UPregulated and DOWNregulated gene-sets (False discovery rate (FDR)<25%) in the tumouroid lines and paired tissues. Full list of gene-sets and significantly enriched gene-sets can be found in Suppl. dataset 2 and 3. **(e)** Schematic of the tumouroid signature. Venn diagram overlapping the upregulated genes in each tumouroid line compared to healthy organoids. **(f)** Table summarizing the results of the gene expression patterns (OE, overexpression) and outcome prediction (KM, Kaplan-Meier) analyses performed for the top genes of the tumouroid signature using publically available TCGA cohorts. The table details the p-values obtained for each analysis (OE in PLC, two-sided t-test ; KM analysis, log-rank test). p-value≤0.05 are defined as significant and color coded using yellow in the table. Only top the 25 genes are represented (Top 30 genes analysis and corresponding values can be found in Suppl. dataset 1). TCGA-HCC, 374 tumoural /50 normal samples; TCGA-CC, 31 tumoural /8 normal samples. **(g)** Box plots for the expression of *STMN1*, *C1QBP* and *C19orf48* in tumoural and normal tissues using the TCGA-HCC and/or CC cohorts. **(h)** Kaplan-Meier analyses in the TCGA-HCC and/or TCGA-CC cohorts based on the expression level of the gene of interest (*STMN1*, *C1QBP* and *C19orf48*) in the tumoural samples.

Figure 4: Tumouroids recapitulate the genetic alterations present in the patient's tumour.

(a) Ploidy analysis of tumouroid cultures expanded for at least 2 months in culture. Results are expressed as % of ploidy per number of metaphases counted (at least 25 total). Healthy-derived organoids were used as control. Experiment was performed at least in duplicate. **(b)** Representative images of organoid metaphases used for the ploidy analysis. **(c-g)** All somatic variants identified in all samples (21 total; 7 patients with 3 samples (Tissue/early organoid/late organoid)) were used for the global analyses after filtering for quality control as detailed in methods (c-e). For f-g, an additional filtering step was applied: a cancer related set of variants was defined by adding the following filtering steps: (1) SNVs, which were included in dbSNP were excluded, with the exception of those which were also included in COSMIC database (resultant variants are detailed in Fig. 4f and Suppl. Fig. 5b). (2) Synonymous SNVs were filtered out as were assumed to be unlikely involved in cancer. (3) A last filtering step was performed selecting for variants present in a panel of genes described in literature to be involved in cancer (847 cancer related genes total, for details see Suppl. Dataset 4). Resultant variants are provided in Suppl. Dataset 4 and were used to select relevant mutations described in Figure 5g. **(c)** Correlation heat-map between PLC-tissues (_T) and PLC-tumouroids (_O) variants identified. **(d)** Proportions of somatic variants across the samples, the 6 types of SNVs and the indels are represented. **(e)** Percentage of the 6 types of SNVs averaged across all samples (21 total; 7 patients with 3 samples (Tissue/early organoid/late organoid samples)). Graph represents mean±SD. **(f)** Bar plots indicate the concordance between the cancer related somatic variants identified in the tumour-of-origin and the corresponding tumouroids expanded for short or long term in culture. **(g)** Genes

altered in tumouroid cultures and associated tissues and known to be mutated in liver OR gastrointestinal tumours. The type of mutation is indicated in the legend. OxS, oxidative stress.

Figure 5: PLC tumouroids recapitulate patient's PLC tumour subtype and metastasis *in vivo* when transplanted in mice.

(a) Experimental design. PLC tumouroids or Healthy liver-derived organoids expanded for >3 months in culture were transplanted subcutaneously (SC) or under the kidney capsule (Kid.Cap.) of immunocompromised NSG mice and analysed for the presence of tumour growth and metastasis following grafting. **(b-c)** Tables summarizing the number of cells, site of engraftment and analysis of tumour and lung metastasis. No tumour lesions were found in any of the mice receiving Healthy-1 organoids. Tumours were dissected at 1 (CC-1_O and Healthy-1_O) and 5 (HCC-1_O and Healthy-1_O) months (SC graft) and 0.5, 1, 2 and 3 months (Kid.Cap. graft) after injection. **(d)** Representative H&E staining of CC-1 tumouroids transplanted subcutaneously (top) into NSG mice and corresponding CC-1 patient's tumour sample (bottom). Note that the grafted CC-1 tumouroids tissue (top) recapitulates the histo-architecture of the patient's original tumour (bottom) including the extensive desmoplasia found on the CC-1 original sample (arrowheads). Scale bars, top left 250µm, top right 125µm, bottom left 125µm, and bottom right 62.5µm. **(e)** Representative H&E staining of HCC-1 tumouroids transplanted subcutaneously (top) into NSG mice and corresponding HCC-1 patient's tumour sample (bottom). Note that the grafted HCC-1 tumouroids tissue (top) recapitulates the histo-architecture of the patient's original tumour (bottom) including the pseudoglandullar rosettes, hallmark of HCC-1 original sample (dashed circle). Scale bars, left 125µm, right 62.5µm. **(f)** Representative H&E (left) and KRT19 (right) immunohistochemistry analyses of CC-1 tumouroids transplanted under the kidney capsule of NSG mice. Scale bars, 125µm. **(g)** Lung metastases derived from the human CC-1 tumouroids transplanted under the kidney capsule cells (right panels) were identified using a human specific KRT19 antibody. No metastases were found in the lungs of mice transplanted with Healthy-1 organoids (left panels). Scale bars, 500µm, magnification 125µm.

Figure 6. PLC tumouroid lines are a valuable resource for drug screening and allowed identification of ERK as a potential target for primary liver cancer.

(a) Scatterplot of 1-AUC values from two biological replicates of the drug screening data, highlighting drugs inducing a viability effect in five liver tumouroid lines. Each data point is the 1-AUC value for a given drug in a particular tumouroid line. **(b)** Dose-response curves after 6 days treatment with Gemcitabine, Nutlin-3a, LGK974 and SCH772984 generated from the luminescent signal intensities. Data displayed are average of the technical and biological replicates. **(c)** Summary of the different drugs used in the drug screening, the associated pathway and nominal targets and the screen results represented as a summary of the the 1-AUC and IC50 data generated for the different tumouroid lines. Red, IC50 within the screen range; Dense dotted pattern, 1-AUC>0.15 and dose response; scattered dotted pattern, 1-AUC>0.15 and sensitivity at highest value only. Compounds highlighted in yellow were selected for further validation. **(d)** Validation of viability effects of a subset of compounds using an organoid formation assay (see details in methods). **(e)** *In vivo* activity of SCH772984 in CC-1_O tumouroids grafted under the skin of NSG mice. Mice were treated with drug/vehicle twice daily for 20 days (n=5 in 2mg/kg of SCH772984 group, n=8 in vehicle group). From day 7 onwards, significant differences between the SCH772984 and the vehicle treated groups were observed. *, p-value<0.01; **, p-value<0.002 (Mann Whitney test, two-

tailed). Results are shown as percentage of the tumour volume relative to day 0 (mean ±SD). **(f-g)** Histological analysis of the antitumor efficacy of SCH772984 on CC-1_O tumors was assessed 24 days after starting the treatment. Representative **(f)** H&E and **(g)** TUNEL staining performed on tissue sections from CC-1_O tumours treated with either vehicle (left) or SCH772984 (right). Representative images from 2 independent experiments are shown. Scale bar, 125µM (H&E) and 25µM (TUNEL).

Supplementary Figure 1: Isolation and culture of human primary liver cancer-derived organoids.

We successfully established and expanded human PLC-derived organoids from 7 different PLC patients, including poorly to moderate/well differentiated HCC (n=2), CC (n=3), and combined HCC/CC (CHC; n=2) by adapting the protocol to isolate and expand liver stem/progenitor cells (Huch et al, 2015) for the timing of tissue digestion (2-3 hours to overnight (O/N) according to the degree of liver fibrosis in the liver biopsy), for the starting culture conditions (tumouroid specific isolation medium (IM)) and closely monitoring the developing organoid structures (in classical IM, healthy organoids might arise, depending on the type of biopsy/resection. In those cases, these are hand-picked upon visual inspection). MWP, multi well plate; ROCKi, Rho kinase inhibitor (Y-27632).

Supplementary Figure 2: Patient-derived PLC organoid cultures expand long term *in vitro*.

(a) Tissues (top row) and tumouroids (middle and bottom rows) obtained from HCC-2, HCC-3, CHC-2, CC-2 and CC-3 patients. H&E staining of the tumoural tissues (top), brightfield (middle) and H&E staining (bottom) pictures of tumouroids originated from the corresponding tissues. Scale bars, 125µm (top), 200µm (middle) and bottom 40µm, 125µm, 125µm, 125µm and 70µm (left to right, respectively). **(b-f)** Representative Ki67 nuclear staining performed on patient's tissues included in the study: **(b)** moderately differentiated HCC (HCC-1,-2), poorly differentiated HCC (HCC-3), **(c)** CHC (CHC-1 and CHC-2), **(d)** moderately differentiated CC (CC-1,-2) and poorly differentiated CC (CC-3), **(e)** well differentiated HCC (wHCC-8) and **(f)** well differentiated CC (wCC-1). Scale bars, 125µm. **(g)** Ki67-labelling index in PLC tissue samples. The percentage of tumour cells that are positive for nuclear Ki67 labelling was determined by counting a minimum of 1000 cells per patient in at least 2 independent slides. Graph represents mean±SD. **(h)** Brightfield pictures of long-term expanded tumouroid cultures. Scale bar, 200µm.

Supplementary Figure 3: Immunohistochemistry and gene expression analyses reveal that the PLC tumouroids retain expression patterns of the distinct subtype of the original tumour they derived from.

(a) IHC analysis for the hepatocyte/HCC marker HepPar1 and the ductal/CC marker EpCAM on CC-3 tissue (_T). Scale bar, 125 µm. **(b-c)** Gene expression analysis (q-RT-PCR) of **(b)** ductal *EPCAM* and **(c)** progenitor *SALL4* genes in both tumour tissues and respective tumouroid lines. q-RT-PCR data are normalized to the expression of the housekeeping gene *HPRT*. Graph represents mean±SD of at least 2 independent experiments. **(d)** PAS-diastase staining on tumoural tissues. Arrowheads mark positive PAS-diastase staining in CHC-1, CC-1 and CC-3 tissues (_T). Scale bar, 62.5 µm.

Supplementary Figure 4: Gene expression, immunohistochemistry and functional analyses reveal that the tumouroids retain the differentiation state of their original tissue, even after long-term expansion in culture.

(a) Representative GSEA plots for 2 gene-sets associated with PLC differentiation [HCC with hepatocyte differentiation features (Hoshida et al., 2009) and cholangiocarcinoma (Andersen et al., 2012)] enriched in the tumouroid lines (_O). +, significantly upregulated; -, significantly downregulated and ns, non significant (FDR>25%). **(b)** IHC of the ductal/CC marker KRT19 in tissues. Scale bar, 125 µm. **(c)** Representative GSEA plots for 1 gene-set describing genes positively correlated with KRT19 expression (Govaere et al., 2013) significantly up or down regulated in the tumoural tissues (_T). +, significantly upregulated; -, significantly downregulated. **(d)** IF analysis for the ductal/CC marker KRT19 (in green) and the hepatocyte markers ALB and HFN4A (in red) on tumouroids expanded in culture for at least 3 months. Nuclei were counterstained with Hoechst33342. Scale bar, 30µm. **(e)** Albumin secretion was assessed by ELISA in the supernatant from HCC and CHC tumouroids. **(f)** Total bile acid production determined by colorimetric assay in HCC tumouroids. **(g)** Gene expression analysis (q-RT-PCR) of the ductal gene *KRT7* in both tumour tissues and respective tumouroid lines. q-RT-PCR, data values are normalized to the expression of the housekeeping gene HPRT. All graphs represents mean±SD of 2 independent experiments.

Supplementary Figure 5: Tumouroids recapitulate the genetic alterations present in the original tumour.

(a-b) WES analysis of patient's tumoural tissues and corresponding tumouroid cultures expanded for < 2 months (early passage) or >4 months (late passage) in culture. All somatic variants identified in all samples (21 total; 7 patients with 3 samples (Tissue/early organoid/late organoid)) were used for the global analyses after filtering for quality control as detailed in methods (a). For (b) an additional filtering step was applied: a cancer related set of variants was defined by adding the following filtering steps: (1) SNVs that were included in dbSNP were excluded, with the exception of those also present in COSMIC database. **(a)** Percentage of the 6 types of SNVs on transcribed and non-transcribed strand averaged across all samples. Graph represents mean±SD. **(b)** Summary table describing the somatic acquired alterations present in all 3 samples per patient (tissue, tumouroids early and late passage) (see details in methods). The median, mean, minimum (min) and maximum (max) number of alterations across patients are indicated. **(c)** Representative GSEA plots for 1 gene-set describing genes up-regulated in tumours developed by transgenic mice overexpressing an EGF secreted form in liver (Borlak et al., 2005) significantly positively enriched in some of the tumouroid lines (_O). +, significantly positively enriched (FDR<25%, p-value<0.05); ns, non significant (FDR>25%). **(d)** Tumouroids cultures were tested for their sensitivity to porcupine inhibitor IWP2 (3 µM). Representative bright field microscopy images (1 out of 3 independent experiments). Scale bars, 500um and 100 um (insets). **(e)** Gene expression analysis (q-RT-PCR) of the Wnt target genes *TNFRSF19, AXIN2* and *LGR5* on IWP2 treated cultures. Gene expression was normalized against a housekeeping gene (*HPR*T) and fold change was calculated relative to the expression on the vehicle-treated control (DMSO control). Significant differences in Wnt target genes expression between IWP2 and vehicle treated conditions were observed, *p-value<0.05 (t-test, two-tailed). Graph shows mean±SD of 2 independent experiments.

Supplementary Figure 6: Transplantation of PLC tumouroids in immunodeficient mice.
(a) CC-2 and CC-3 tumouroids expanded for at least >3 months in culture were transplanted subcutaneously (posterior flanks) on immunocompromised NSG mice and analysed for the presence of tumour growth. Table summarizing the number of cells, site of engraftment and analysis of tumour in the different mice. **(b-c)** Representative images of tumouroids transplanted **(b)** under the skin (SC) or **(c)** under the kidney capsule (Kid.Cap.) of immunodeficient mice. Scale bar, 2 mm. **(d)** Representative H&E staining of CC-2 tumouroids transplanted subcutaneously (SC) into NSG mice and corresponding CC-2 patient's tumour tissue (bottom). Scale bars, 125µm (black), 62.5µm (inset). **(e)** Ki67 staining on xenografts developed under skin (SC) revealed that the tumours were highly proliferative. Scale bar, 125µm (top), 62.5µm (magnification). Similar data was obtained on xenografts developed under kidney capsule (data not shown). **(f)** Lung metastasis were found on mice transplanted with CC-1 tumouroids under the kidney capsule. Scale bar, 2mm. Magnification 2x. **(g-h)** Tumouroids were re-derived and expanded from tumours derived from CC-1 tumouroids transplanted into the kidney capsule (Kid.Cap.) or HCC-1 tumouroids transplanted subcutaneously (SC) into immunocompromised NSG mice. **(g)** Representative brightfield and H&E staining images obtained after 5 passages in culture. Scale bar, 500µm (brightfield, top left), 200µm (brightfield, top right) and 125µm (H&E staining). **(h)** Ploidy analysis of CC-1 and HCC-1 tumouroids rederived from xenografted tumours. Number of metaphases counted, CC-1_O_Kid.Cap.#1, n=15; CC-1_O_Kid.Cap.#2, n=16, HCC-1_O_SC#1, n= 12. Experiment was performed at least in duplicate. Note that morphology, histology and chromosome counts are maintained when comparing the parental tumouroids (derived directly from patient's tumour) and the tumouroids rederived after xenografting.

Supplemental Figure 7: PLC tumouroid lines can be used to identify gene-drug associations that may facilitate personalized therapy.
(a) Scatterplot of area under the dose-response curve (AUC) values obtained for the drugs that were used to validate the drug screening using the tumouroid formation assay presented in Fig.6d (Gemcitabine, Taselisib, Dasatinib, AZD8931 and SCH772984). Plots show the correlation between the two biological replicates for each tumouroid line and each data point represents the area under the dose-response curve (1-AUC) value. Red, sensitive. Triangle, result further validated in the tumouroid formation assay. **(b)** Organoid cultures derived from Healthy-1, HCC-1 and CC-1 tissues were tested for their sensitivity to treatment with the EGFR inhibitor Gefitinib (1µM). Representative brightfield microscopy images (1 out of 2 independent experiments). Note that, CC-1 organoids were resistant to the treatment, while Healthy-1 and HCC-1 organoids were sensitive, in agreement with their mutation profile (see Fig. 4). Scale bars, 500µm and 100µm (insets). **(c)** GSEA analyses comparing tumouroid's and tissue's gene expression signatures to 159 curated gene-sets associated with liver cancer and stem cell. Representative GSEA plots obtained for a gene-set describing genes overexpressed upon TGFB1 treatment (Coulouarn et al., 2008) and significantly upregulated (FDR<25%, pvalue<0.05) in CC-2 patient's tumouroid line and original tissue. +, significantly upregulated. **(d)** *In vivo* activity of SCH772984 in HCC-1_O tumouroids grafted under the skin of NSG mice. Mice were treated with drug/vehicle twice daily for 15 days (n=3 in 2mg/kg of SCH772984 group, n=2 in vehicle group). Significant differences between the SCH772984 and the vehicle treated groups were observed. *, p-value<0.01 and **, p-value<0.002 (t-test, two-tailed). Results are shown as percentage of the tumour volume relative to day 0 (mean ±SD). **(e)** Histological analysis of the antitumour efficacy of SCH772984 on HCC-1_O tumours. Representative H&E stainings on tissue sections from

HCC-1_O tumours treated with either vehicle (left) or SCH772984 (right). Representative images of 2 independent experiments are shown. Scale bar, 125uM. **(f-g)** Western blot analysis for phosphorylated ERK1/2 (P-ERK) and total ERK (ERK) in either **(f)** tumouroids in culture or **(g)** CC-1 xenografted tumours. **(f)** HCC1 and CC-1 tumouroid line (_O) were treated for 24 hours with either the pan-ERBB inhibitor AZD8931, the pERK inhibitor SCH772984 or with the vehicle and samples were collected for western blot analyses as described in methods. AZD8931 reduced ERK phosphorylation in HCC-1_O line only, whereas SCH772984 potently inhibited ERK phosphorylation in both HCC-1_O and CC-1_O lines, as expected according to their mutational profile (HCC-1_O, KRAS WT and CC-1_O, KRAS G12D; see Figure 4). Representative blots of 2 independent experiments are shown. **(g)** Target engagement of SCH772984 on phosphorylated ERK in CC-1 tumours grafted under the skin of NSG mice. Tumours were dissected 6 hours after injecting SCH772984 (2mg/kg) or vehicle intratumourally. Homogeneates from these were obtained as described in methods and probed to assess phosphorylated ERK1/2 (P-ERK) and total ERK (ERK) levels. Representative blots of 2 independent experiments are shown.

Supplementary Table 1: Patients' information and organoid efficiency derivation and expansion.

Table summarizing all the patient's and healthy donor information including gender, age, type of tissue, histological analysis, Ki67 index and serum AFP levels. Organoid growth and expansion are indicated when appropriate. Efficiency of derivation and efficiency of organoid expansion are calculated. Note that all healthy tissues derived from healthy donors undergoing liver transplantation. N/A, not applicable; N/T, not tested.

*Organoids from HCC-NL1 patient (derived at Erasmus Rotterdam Centre) became contaminated after some weeks in culture, and therefore were excluded from the analysis

Supplementary Dataset 1: RNAseq data analysis.

Dataset including S1-S7 tables summarizing all the RNAseq data analyses except GSEA (see Suppl. Dataset 2 and 3) and the TCGA analysis. Used for Fig.3.

Supplementary Dataset 2: Tumouroids GSEA data.

Dataset including S1-S15 tables summarizing the tumouroids GSEA data used for Fig. 3 and Suppl. Fig. 4, 5 and 7.

Supplementary Dataset 3: Tissue GSEA data.

Dataset including S1-S15 tables summarizing the tissues GSEA data used for Fig. 3 and Suppl. Fig. 4, 5 and 7.

Supplementary Dataset 4: WES.

Dataset including S0-S8 tables summarizing the cancer-related variants found in short (early) and long (late) term expanded cultures and corresponding tissues used for Fig. 4g.

Supplementary Dataset 5: Drug screening.

Dataset including S1-S2 tables summarizing the List of drugs screened, their concentration and the data used for Fig. 6 and Suppl. Fig. 7

Supplementary Dataset 6: List of antibodies, kits, and primers used. List of drugs screened.

METHODS

Human specimens

Liver tumour biopsies (~1cm^3) were obtained from biopsies or resection performed at Erasmus Medical Center Rotterdam MEC-2013-143, Cambridge University Hospitals NHS Trust REC: 15/LO/0753 (Approval by NRES Committee London – Westminster) and The Royal Infirmary Hospital Edinburgh REC: 15/ES/0097. Healthy livers biopsies (~1cm^3) were obtained during liver transplantation performed at the Erasmus Medical Center, Rotterdam MEC-2014-060 and at the Cambridge University Hospitals NHS Trust REC: 15/EE/0152. The Cambridge samples were provided by the Cambridge Bioepository for Translational Medicine (CBTM). All patients provided informed consent. Samples were procured and the study was conducted under Institutional Review Board approval prior to tissue acquisition. Samples were confirmed to be tumour or normal based on histopathological assessment. The diagnosis of each case was confirmed on routine hematoxylin and eosin-stained slides by an independent histopathologist.

Isolation and Culture of human liver healthy and tumoural organoids

Healthy liver-derived were isolated and cultured using our previously described method [23, 24] while tumour-derived organoids (tumouroids) were isolated by adapting this method as follows. Tissue (~1cm^3) was minced and incubated at 37°C with the digestion solution for 2-3 hours to overnight (O/N) according to the degree of liver fibrosis in the liver biopsy. The digestion was stopped once no pieces of tissue were left, and the suspension was then filtered through a 100µm nylon cell strainer and spun 5 min at 300-400G. The pellet was washed in cold Advanced DMEM/F12 (GIBCO) then mixed with BME (Basement Membrane Extract, Type 2, Pathclear). 10,000-30,000 cells were seeded per well in a 24-multi-well plate. After BME had solidified, half of the wells obtained for each sample was cultured in the classical human liver organoid isolation medium (Advanced DMEM/F12 supplemented with 1% Penicillin/Streptomycin, 1% Glutamax, 10 mM HEPES, 1:50 B27 supplement (without Vitamin A), 1:100 N2 supplement, 1.25mM n-Acetylcysteine, 10% (vol/vol) Rspondin-1 conditioned medium, 30% (vol/vol) Wnt conditioned medium, 10mM nicotinamide, 10nM recombinant human [Leu15]-Gastrin I, 50ng/ml recombinant human EGF, 100ng/ml recombinant human FGF10, 25ng/ml recombinant human HGF, 10µM Forskolin, 5µM A83-01, 25ng/ml Noggin and 10 µM Y27632 as described in [23, 24]). The other half was cultured in a tumouroid specific isolation medium (classical human liver organoid isolation medium (see above) without Noggin and Rspo1 and Wnt conditioned media but supplemented with 3nM Dexamethasone (Sigma Aldrich)). These media were kept until the first split (2-3 weeks after isolation) then, changed into a classical human complete medium (Advanced DMEM/F12 supplemented with 1% Penicillin/Streptomycin, 1% Glutamax, 10 mM HEPES, 1:50 B27 supplement (without Vitamin A), 1:100 N2 supplement, 1.25mM n-Acetylcysteine, 10% (vol/vol) Rspondin-1 conditioned medium, 10mM nicotinamide, 10nM recombinant human [Leu15]-Gastrin I, 50ng/ml recombinant human EGF, 100ng/ml recombinant human FGF10, 25ng/ml recombinant human HGF, 10µM Forskolin and 5µM A83-01 as described in [23, 24]). Medium was changed twice a week. For tumouroid culture establishment, after 2-3 weeks in culture (depending on the sample) the growing structures were visually inspected and, if required, contaminating healthy organoids were hand-picked to prevent these from outgrowing the tumouroid structures. Upon attainment of dense culture, passaging was

performed by mechanical dissociation into small fragments via trituration with a glass Pasteur pipet, and transferred to fresh matrix in complete medium (composition described above).
To prepare frozen stocks, organoid cultures were dissociated and mixed with recovery cell culture freezing medium (GIBCO) and frozen following standard procedures. When required, the cultures were thawed using standard thawing procedures and cultured as described above. For the 3-4 days (organoids) or first 2 weeks (tumouroids) after thawing, the culture medium was supplemented with Y-27632 (10μM). Organoid pictures were taken with either a Leica M80 stereoscope and Leica MC170 HD camera or with an inverted microscope Leica DMIL and Leica DFC 450C camera.

Histology and staining

Tissues and organoids were fixed for 24 or 0,5 hours respectively, in 10% neutral buffered formalin (Sigma), at room temperature, and then embedded in paraffin as follows: briefly, tissues were processed through a graded ethanol series followed by xylene, and then embedded in paraffin, cut at 5μm and stained (H&E and immunohistological staining). For immunofluorescence experiments fixed organoids were rehydrated with PBS following formalin fixation. For immunohistological staining, paraffin slides were deparaffinised and subjected to antigen retrieval using citrate sodium solution pH=6. To reduce background nonspecific staining, and permeabilise the sample, slides were incubated with a 3% BSA, 0,5% Triton in TBS solution for 1 hour. Primary antibodies (listed in the Suppl. Dataset 6_S1) were then applied at appropriate dilutions for overnight at 4°C (see Suppl. Dataset 6_S1 for details). Endogenous peroxidase activity was blocked for 15 min in a 3% hydrogen peroxide/methanol buffer. Detection of bound antibody was accomplished with the BrightVision Ultimate kit (Immunologic). Briefly, slides were washed in TBS and incubated with a secondary antibody-HRP conjugate for 1hour at room temperature and finally developed with 3,3′-diaminobenzidine (DAB) for 5 min, counterstained with hematoxylin, and mounted with DPX (Sigma). Slides were also stained in the absence of primary antibodies to evaluate nonspecific secondary antibody reactions. For TUNEL assay, Click-iT Plus TUNEL kit (Molecular Probes, Life technologies) was used in accordance with the manufacturer's instructions. Pictures were taken with a Leica microscope DM 4000 microscope and DFC 450 camera (Leica). For whole mount immunofluorescence staining, organoids were processed as described in [22, 23] [24]. Briefly, organoids were incubated over 2 to 3 night at 4°C, washed in PBS, and revealed by incubation with a secondary antibody conjugated to a fluorophore. Nuclei were stained with Hoechst33342 (Molecular Probes, Life technologies). Confocal images were captured on a Leica SP5 inverted confocal microscope (Leica).

Ki67 index

Each tumour slide stained for Ki67 was manually scanned with a microscope at × 10 objective, and the area of greatest Ki67 positivity (hot spot) was selected for photographing. At least 1000 total tumoural cells were counted on a total of 2 independently stained slides per patient. Pictures were taken with a Leica microscope DM 4000 microscope and DFC 450 camera (Leica) and Ki67-negative and -positive were then counted using ImageJ "cell counter" plugin. Light brown or pale staining nuclei were ignored during counting.

Karyotyping

Karyotyping was performed as previously described [23]. Briefly, cultures were incubated with 0.1ug/ml Karyomax Colcemid (Gibco). After 24 hours, organoids were harvested and dissociated using TrypLE (Gibco). Cells were incubated with KCL 0.0075M hypotonic solution for 10 min, fixed in methanol:acetic acid (3:1) and dropped on a microscope slide for visualization. Nuclei were mounted and stained using Vectashield with DAPI (Vector Labs). A minimum of 15 metaphases per sample were counted.

Sequencing and analysis

For both RNA-Sequencing (RNASeq) and Whole-Exome Sequencing (WES), low quality reads were filtered (<Q20) followed by trimming of low quality bases from the ends of the reads (<Q20). Adaptors were also removed using cutadapt.

RNA-Sequencing. RNA was isolated from organoids using RNeasy mini kit (Qiagen) following manufacturer's instructions. RNA libraries were prepared for sequencing using the Smartseq2 method. RNA sequencing was performed using Illumina HiSeq sequencer (50bp single-end reads and 10-20 million reads were generated for each sample). Reads were aligned with Tophat (v2.1.0) [67] to the GRCh38.82 genome, using the corresponding gtf file for exon positions. Counts were generated using featureCounts (v1.5.0-p1) [68]. Only protein-coding genes, lincRNAs, processed transcripts and misc RNA were kept for further study. Normalised counts were created using DESeq2 [69] and RPKMs using edgeR's function [edgeR]. The technical and biological replicates were merged. To assess concordance of tissues with organoids genes were filtered and the Pearson's correlation coefficient was calculated pairwise between tissues and organoids. The correlation matrix was then z-scored. The principal components for several subgroups of the samples were calculated from the normalised DESeq counts, and the first two (PC1, PC2) were plotted. We then analysed the top 100 genes with highest loadings across PC2, which separated the samples by subtype. Functional analysis was split across the three subtypes, and genes were excluded in each unless healthy or tumour samples had RPKM values greater than 1. To generate a statistic for tumoural tissue samples, the log2 fold change (FC) of each tumoural tissue was divided by the mean of the healthy tissues. To generate a statistic for HCC tumouroid samples, two log2 fold changes (FC) were calculated: the first was HCC organoid divided by the mean of healthy liver-derived organoid and the second was HCC tissue divided by the mean of the healthy tissues. Then the mean or minimum was then taken of these two ratios, whichever had a lower absolute value. The same statistic was generated for CHC and CC tumouroids using the mean healthy tissue instead of healthy liver-derived organoid as a baseline for the first fold change. These statistics were then used for pre-ranked gene set enrichment analysis using GSEA software (http://www.broadinstitute.org/gsea/) [70]. 159 gene sets were used for running the GSEA. These gene sets were obtained after curation of the publically available C2 MSigDB collection for "LIV", "HEPT" and "STEM" key words and completed by available liver cancer gene set described in literature (see Supplementary Dataset 2 and 3) in order to select a relevant list of gene sets associated with liver cancer and stemness. 1,000 permutations were used to calculate p-value. A tumouroid signature was identified by finding genes with the highest FC when dividing the minimum expression value, in RPKMs, over all tumouroid samples by the mean of the expression of healthy liver-derived organoids in differentiation medium. Several aspects of the genes defining the tumouroids' signatures were annotated: the description of their corresponding proteins was downloaded

from Uniprot [71], and their relevance to disease by retrieving the Disease Ontology terms (using the R package dnet v1.0.10 [72]).

WES. DNA from tumour tissue and matched tumouroid lines was extracted using DNeasy Blood & Tissue Kit (Qiagen) according to manufacturers' protocol. Somatic point mutations and short indels were called in a procedure composed of several steps as follows: **(i)** Reads were aligned to the UCSC hg38 genome using Bowtie2 (v2.2.6) [73] and the output was preprocessed for variant calling by marking duplicates with Picard (v1.113) (http://broadinstitute.github.io/picard/) followed by Indel realignment with the GATK toolkit (v3.7) [74]. SNPs and Indels were called with Varscan (v.2.3) [75]. **(ii)** We identified and selected the variants with the following parameters: base quality ≥15 (Phred score), read depth ≥15 and annotated by SNPEff [76] as not "intergenic". **(iii)** We removed SNPs on alternate haplotypes. **(iv)** Analysis was then split between patients. For each, there were 3 samples, the tissue and the corresponding tumouroids expanded for <2months (early) or >4months (late). If a SNV was called in the 'early' sample, a SNV was added in the tissue if its pileup showed evidence of the same variant at that position. Moreover if a SNV was called in the 'late' sample, a SNV was added in the tissue and early sample if their pileup both showed evidence of the same variant at that position. Figure 4c-e and Suppl. Figure 5a are based on this final list of somatic variants. To assess concordance, overlaps of SNVs found in tissue and early and late tumouroids were calculated within and between cancer types using GATK (v3.7). The mutation spectrum was examined in each sample in both non-transcribed and transcribed strands and then summarized by representing the average proportion across all samples. A cancer related set of variants was defined by adding the following filtering steps: **(v)** SNVs which were included in dbSNP (v150) [77] were excluded, with the exception of those which were also included in COSMIC (v76) [78]. The variant positions with their associated effects were annotated with SnpEff. Figure 4f is based on this final list of somatic variants. A summary of the concordant (tissue/early/late) variants obtained per patient is provided in Suppl. Figure 5b. **(vi)** Synonymous SNVs were filtered out as were assumed to be unlikely involved in cancer. **(vii)** A final filtering step was performed selecting for variants present in a panel of genes created based on literature (847 genes described in cancer). Resultant variants are provided in Suppl. dataset 4 and were used to find relevant mutations described in Figure 5g.

Accession Numbers

All RNA-seq and WES data are available at Gene Expression Omnibus (GEO) under accession number GSE84073.
https://www.ncbi.nlm.nih.gov/geo/query/acc.cgi?acc=GSE84073

The Cancer Genome Atlas (TCGA) analyses

We examined the expression of the top 30 genes of this tumouroid signature, in public available data generated by the TCGA Research Network: http://cancergenome.nih.gov/. FPKMs were downloaded from The Genomic Data Commons Data Portal (GDC), using GDC's API, for the projects TCGA-LIHC (374 tumoral samples (ICD-O-3 number=C22.0) and 50 normal control samples) and TCGA-CHOL (31 tumoral samples (ICD-O-3 number=C22.1) and 8 normal control samples). From the FPKM values of tumoral and control samples we generated base R boxplots and assess the significance between both group

by unpaired two-tailed t-test. Survival plots were created using the R package TCGAbiolinks (v2.2.10) [79] and by splitting, per gene, the tumour samples into high- and low-expression groups. The median of all samples was used as the threshold and significance for differences between the two groups was assessed by log-rank test.

Quantitative RT-PCR

Total RNA was extracted from organoid cultures or freshly isolated tissues using RNeasy mini kit (Qiagen) in accordance with the manufacturer's instructions. cDNA was synthesized using 0.5µg of total RNA and a M-MLV Reverse Transcriptase kit (Promega). cDNA was amplified with iTaq™ Universal SYBR Green Supermix (BioRad) and using gene-specific primers described in Suppl. Dataset 6_S3). All targets were amplified (40 cycles) on a CFX96 Touch Real-Time PCR Detection System (Biorad). Data were analyzed using BioRad CFX manager. Expression levels were normalized to the expression of the housekeeping gene *HPRT*.

Functional *in vitro* studies

Functional studies were performed in collected supernatant or in whole organoids. To assess albumin production, culture medium was collected 1 week after the last medium change and albumin levels were assessed using an Albumin ELISA kit (Assay Pro) according to manufacturer's instructions. Values were corrected for time and cell number. Concentration of total bile acid was established using a Total Bile Assay kit (Cell Biolabs, inc.) according to manufacturer's instructions on supernatant obtained after sonication of whole organoids in PBS.

Organoid formation Assay

To assess the organoid formation efficiency in classical *vs* tumouroid isolation medium, pictures of all full drops of BME obtained per patient were photographed using a Leica M80 stereoscope 2-3 weeks after isolation (depending on the sample) and all viable tumouroid structures were counted.
For the drug sensitivity assays, organoids were dissociated into 2-5 cell clumps by enzymatic dissociation with TrypLE (Life Technologies). Then, cell viability assays were conducted by plating 500 clumps per well of a 48-well cell culture plate in 250µl of complete human medium supplemented with 0.5 µM Gemcitabine (Actavis), or 5 µM of AZD8931 (Selleckchem), or 10µM of SCH772984 (Selleckchem) or 2µM Dasatinib (Selleckchem) or 10µM of Taselisib (Selleckchem) or 3µM of IWP2 (Sigma Aldrich) or 1µM of Gefitinib (Selleckchem) or vehicle (DMSO) control. All conditions were supplemented with Rho kinase inhibitor Y-27632 (Sigma-Aldrich). The concentration selected for each compound was based on the cell viability data from our laboratory, the results from the screening or the literature. Medium was changed 3 times a week for 3 weeks. Viable cells were assessed by their ability to generate organoid *de novo*. Representative pictures of the viability result were taken 2-3 weeks after starting the treatment. All cell viability experiments were conducted at least in duplicate.

Drug screening

Organoid viability assays were conducted as previously described [18, 60]. Briefly, 8µl of ~7mg/ml BME-2 was dispensed in to 384-well microplates and allowed to polymerize. Organoids were mechanically dissociated by pipetting before being resuspended in 2% matrigel/growth media (15,000-20,000 organoids/ml) and dispensed into 384-well plates. The following day a 7-point half-log dilution series of each compound was dispensed using liquid handling robotics and cell viability assayed using CellTiter-Glo® (Promega) following 6 days of drug incubation. Screens were performed in technical (same screening run) and biological duplicates, and all screening plates were subjected to stringent quality control measures and a Z-factor score comparing negative and positive control wells was calculated. Dose–response curves were fitted to the luminescent signal intensities utilizing a method previously described [80]. Variation in replicates was greater than similar screens performed in colorectal tumouroids and was likely due to the large size of HCC tumouroids leading to uneven distribution in screening wells [18, 60]. Compound and screening concentrations are provided in Supplementary Dataset 5_S1. The range of concentrations selected for each compound was based on *in vitro* data of concentrations inhibiting relevant target activity and cell viability based on data from our laboratory or literature.

Mouse xenograft studies

All mouse experiments have been regulated under the Animals (Scientific Procedures) Act 1986 Amendment Regulations 2012 following ethical review by the University of Cambridge Animal Welfare and Ethical Review Body (AWERB). For subcutaneous grafts, 1 million cells suspensions were prepared in PBS-0.1%BSA (CC and healthy liver-derived organoid lines) or in Advanced DMEM/F12 (GIBCO) 1% glycosil (ESI-BIO) further supplemented with 50 ng/ml each of HGF and VEGF (HCC and healthy liver-derived organoid lines) and were injected into both flanks of male NSG-NOD scid gamma mice (Charles River). Visible tumours developed in approximately 2–4 weeks (CC organoid lines) and 4-6 months (HCC-1 organoid line). Mice were culled when the tumour reached limit end-point (size or ulceration). For kidney capsule graft, cell line suspensions were prepared in Advanced DMEM/F12 (GIBCO) with BME2 (7mg/ml) and 500,000 cells were implanted under the renal capsule of NSG mice. These mice were then culled at different time point (0.5, 1, 2 and 3 month) and kidney and lung tissues were harvested to assess the growth and the metastatic potential of the grafted cells.

To assess the efficiency of the ERK inhibitor SCH772984 *in vivo* mice with established subcutaneous tumours were randomized to drug treatment by splitting size-matched tumours in two groups (SCH772984/vehicle). Treatments (SCH772984 at 2 mg/kg, or an equal volume of vehicle (25%DMSO-30%PEG300 in DD water)) were administered by intratumoural injection twice daily for 15 (CC-1 tumouroid line) or 20 (HCC-1 tumouroid line) days. Tumour sizes were measured 3 times a week after the first week of treatment using a caliper and volumes were calculated by applying the formula $v = 0.5 \times L \times w \times h$, where v is volume, L is length, w is width and h is height. Investigators performing tumour measurements were blinded to treatment groups.

Western blot assay

Cell lysate for Western blotting were prepared from tumouroids grown for 24 hours in complete human medium supplemented with 10µM of SCH772984 (Selleckchem), or 5 µM of AZD8931 (Selleckchem) or equal volume of vehicle (DMSO), then washed with ice-cold

PBS to remove the basement matrix and from CC-1 xenografted tumours 6 hours after intratumoural injection of 2mg/kg of SCH772984 (Selleckchem). Lysates were made in ice-cold buffer consisting of 50mM Tris-HCl (pH 7.4), 150mM NaCl, 2mM EDTA, 50mM NaF, 1% triton, 1% NP-40, 0.1% SDS, 0.5% Na-deoxycholate, supplemented with 1mM sodium orthovanadate and protease inhibitor cocktail (Roche) (15min on ice for the cells and 30min on ice for the tissues). Protein lysates were cleared by microcentrifugation at 10,000 rpm for 10 min at 4°C and the supernatants aliquoted and stored at −20°C. Equivalent amounts of protein from each sample were separated on 10% SDS-PAGE gels and then transferred by electroblotting onto nitrocellulose membranes. Membranes were then blocked in in PBS-0.1% Tween-5% BSA and immunoblotted with the following antibodies overnight at 4°C: ERK (1/2000), P-ERK (1/3000) (Cell signalling). After washing 3 times in PBS-0.1% Tween, the membranes were incubated for 1h at room temperature with anti-rabbit horseradish peroxidase (HRP)-conjugated secondary antibodies (1:10,000; abcam). Antibody-protein complexes were visualised using ECL Prime Western Blotting Detection Reagent (GE Healthcare).

Statistical Analyses

All summary data are presented as mean ± SD or representative images of at least 2 independent experiments. All statistical analyses were performed in R and GraphPad Prism software (GraphPad 7.0). Sample size (n) values used for statistical analyses are provided in the relevant figures and supplementary figures. Tests for differences between two groups were performed using Mann-Whitney's two-tailed test, Student's two-tailed unpaired t-test or log-rank test as specified in the figure legends. When using t-test we assumed normality and equal distribution of variance between the different groups. No data points were excluded from the statistical analyses. Significance was set at FDR ≤ 0.25 (for GSEA) and p-value ≤ 0,05 (for all other experiments).

References Methods

67. Trapnell, C., L. Pachter, and S.L. Salzberg, *TopHat: discovering splice junctions with RNA-Seq.* Bioinformatics, 2009. **25**(9): p. 1105-11.
68. Liao, Y., G.K. Smyth, and W. Shi, *featureCounts: an efficient general purpose program for assigning sequence reads to genomic features.* Bioinformatics, 2014. **30**(7): p. 923-30.
69. Love, M.I., W. Huber, and S. Anders, *Moderated estimation of fold change and dispersion for RNA-seq data with DESeq2.* Genome Biol, 2014. **15**(12): p. 550.
70. Subramanian, A., et al., *Gene set enrichment analysis: a knowledge-based approach for interpreting genome-wide expression profiles.* Proc Natl Acad Sci U S A, 2005. **102**(43): p. 15545-50.
71. The UniProt, C., *UniProt: the universal protein knowledgebase.* Nucleic Acids Res, 2017. **45**(D1): p. D158-D169.
72. Fang, H. and J. Gough, *The 'dnet' approach promotes emerging research on cancer patient survival.* Genome Med, 2014. **6**(8): p. 64.
73. Langmead, B. and S.L. Salzberg, *Fast gapped-read alignment with Bowtie 2.* Nat Methods, 2012. **9**(4): p. 357-9.

74. McKenna, A., et al., *The Genome Analysis Toolkit: a MapReduce framework for analyzing next-generation DNA sequencing data.* Genome Res, 2010. **20**(9): p. 1297-303.
75. Koboldt, D.C., et al., *VarScan: variant detection in massively parallel sequencing of individual and pooled samples.* Bioinformatics, 2009. **25**(17): p. 2283-5.
76. Cingolani, P., et al., *A program for annotating and predicting the effects of single nucleotide polymorphisms, SnpEff: SNPs in the genome of Drosophila melanogaster strain w1118; iso-2; iso-3.* Fly (Austin), 2012. **6**(2): p. 80-92.
77. Sherry, S.T., et al., *dbSNP: the NCBI database of genetic variation.* Nucleic Acids Res, 2001. **29**(1): p. 308-11.
78. Forbes, S.A., et al., *COSMIC: exploring the world's knowledge of somatic mutations in human cancer.* Nucleic Acids Res, 2015. **43**(Database issue): p. D805-11.
79. Colaprico, A., et al., *TCGAbiolinks: an R/Bioconductor package for integrative analysis of TCGA data.* Nucleic Acids Res, 2016. **44**(8): p. e71.
80. Vis, D.J., et al., *Multilevel models improve precision and speed of IC50 estimates.* Pharmacogenomics, 2016. **17**(7): p. 691-700.

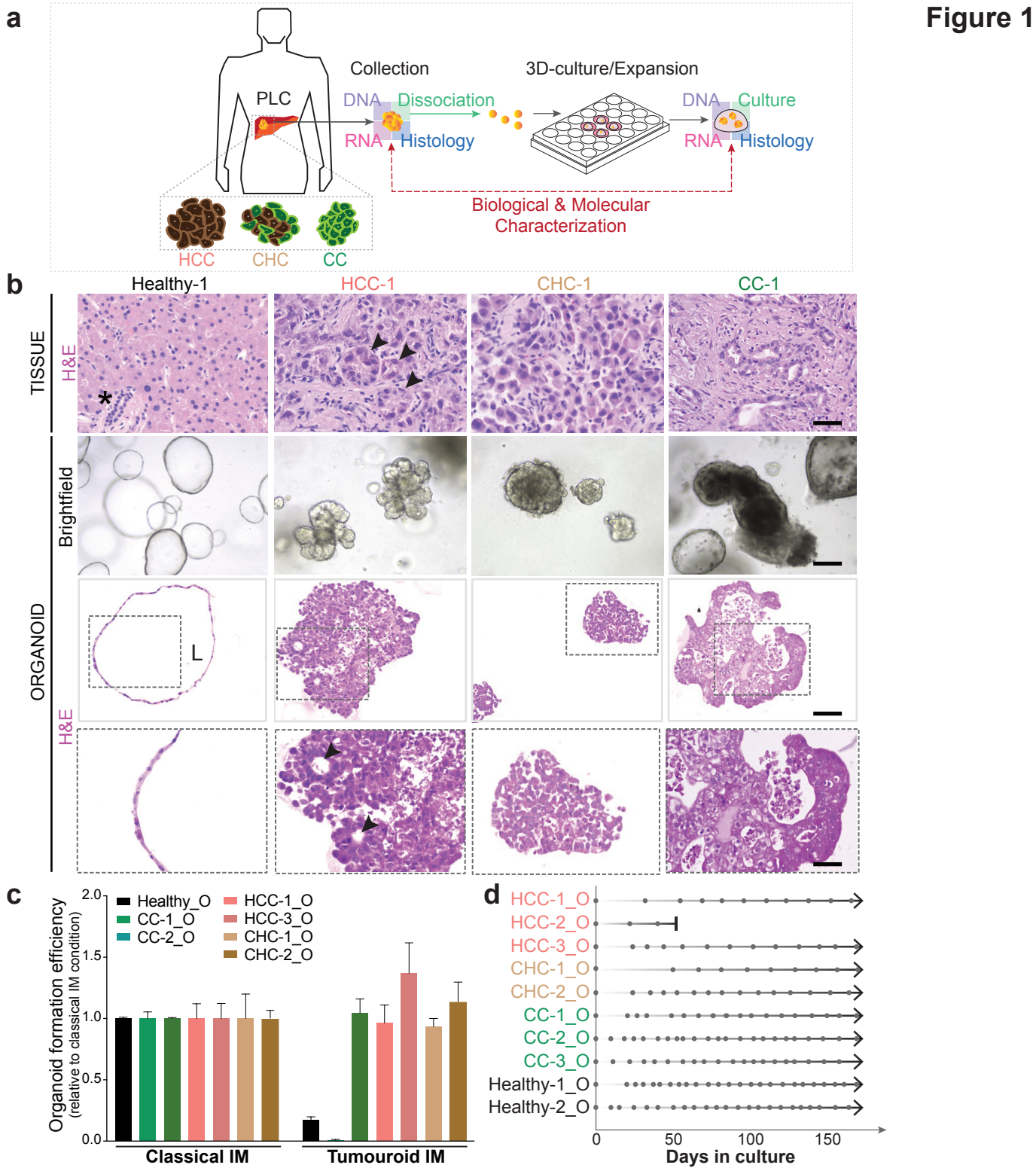

Figure 1: Patient-derived primary liver cancer organoid cultures expand long-term in vitro while preserving the histological architecture of the specific subtype of primary liver tumour they derived from.
(a) Experimental design. For each tissue, samples were split into 4 parts and processed for histology, RNA and DNA isolation, or dissociated and processed for organoid culture. Healthy (donor-derived) liver tissues, moderate/well differentiated hepatocellular carcinoma (HCC), combined hepatocellular-cholangiocarcinoma (CHC) and cholangiocarcinoma samples (CC) were obtained from patients undergoing surgery (patient's information detailed in Supplementary Table 1) and were processed as described in Methods and Suppl. Fig.1. **(b)** Representative H&E staining of healthy liver tissue and primary tumour (top row), and corresponding brightfield microscopy images (middle row) and H&E histological analysis of the organoid lines derived from these (bottom row). Note that, while healthy liver-derived organoids (left) grew as single layered epithelium of ductal-like cells surrounding a central lumen (*, duct; L, lumen), tumour-derived organoids (= tumouroids) formed solid/compacted structures that resembled the corresponding tumour-of-origin [compare tissue (top row) with the corresponding organoid histology (bottom row)]. HCC-1 tumouroids exhibit pseudoglandular rosettes (arrowheads, bottom row), a hallmark of HCC, also found in the parent tumour tissue (arrowheads, top row). CC-1 tumouroids, present a glandular lumen, similar to the original patient's tumour (top row). Scale bars, middle rows 100µm; top and bottom rows, 50µm. Brightfield and H&E pictures from other lines are provided in Suppl. Fig. 2. **(c)** Organoid formation efficiency in classical human healthy liver isolation medium (see Broutier et al, 2016 for details) and tumouroid specific isolation medium (classical human healthy liver complete medium without RSPO + 3nM Dexamethasone - see Methods and Suppl. Fig1 for details). Graph represents mean±SD of the total number of tumouroids obtained per well of each condition. **(d)** Expansion potential of tumouroid cultures established and their correlation to the expansion of healthy-tissue derived organoids. Arrow, continuous expansion. Dot, passage.

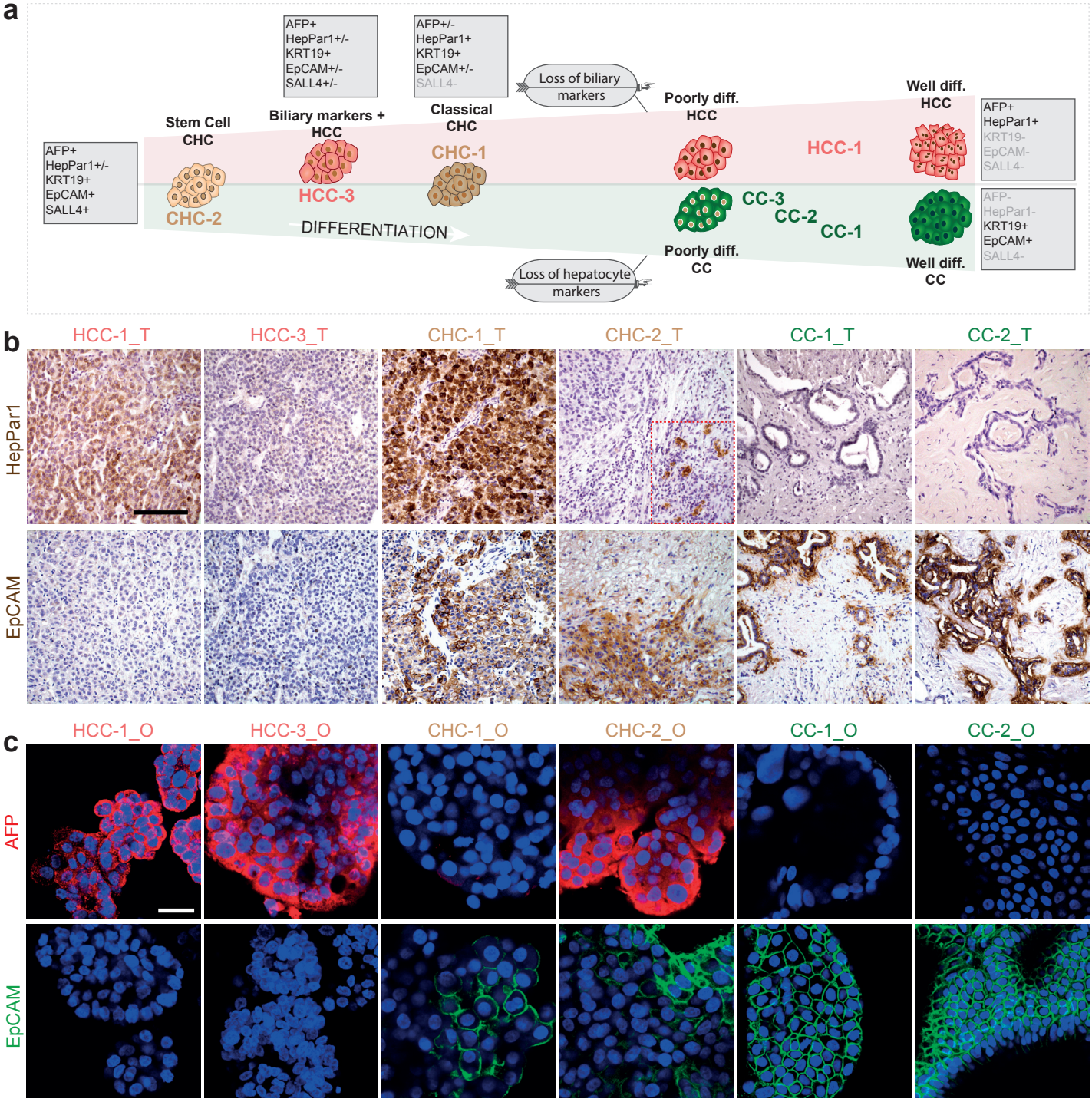

Figure 2: Immunohistochemistry analyses reveal that the PLC tumouroids retain expression patterns of the distinct subtype of the original tissue they derived from, even after long-term expansion in culture.
(a) Schematic representation of the multiple subtypes among types of primary liver cancers (PLC). **(b)** IHC assays on the PLC tissues including hepatocyte/HCC marker (HepPar1) and ductal/CC marker (KRT19). Scale bar, 125 μm. Dashed red square indicates focal staining. **(c)** Immunofluorescent analysis for the HCC marker AFP (in red) and the ductal/CC marker EpCAM (in green), on tumouroids expanded in culture for at least 3 months. Nuclei were counterstained with Hoechst33342. Scale bar, 30μm.

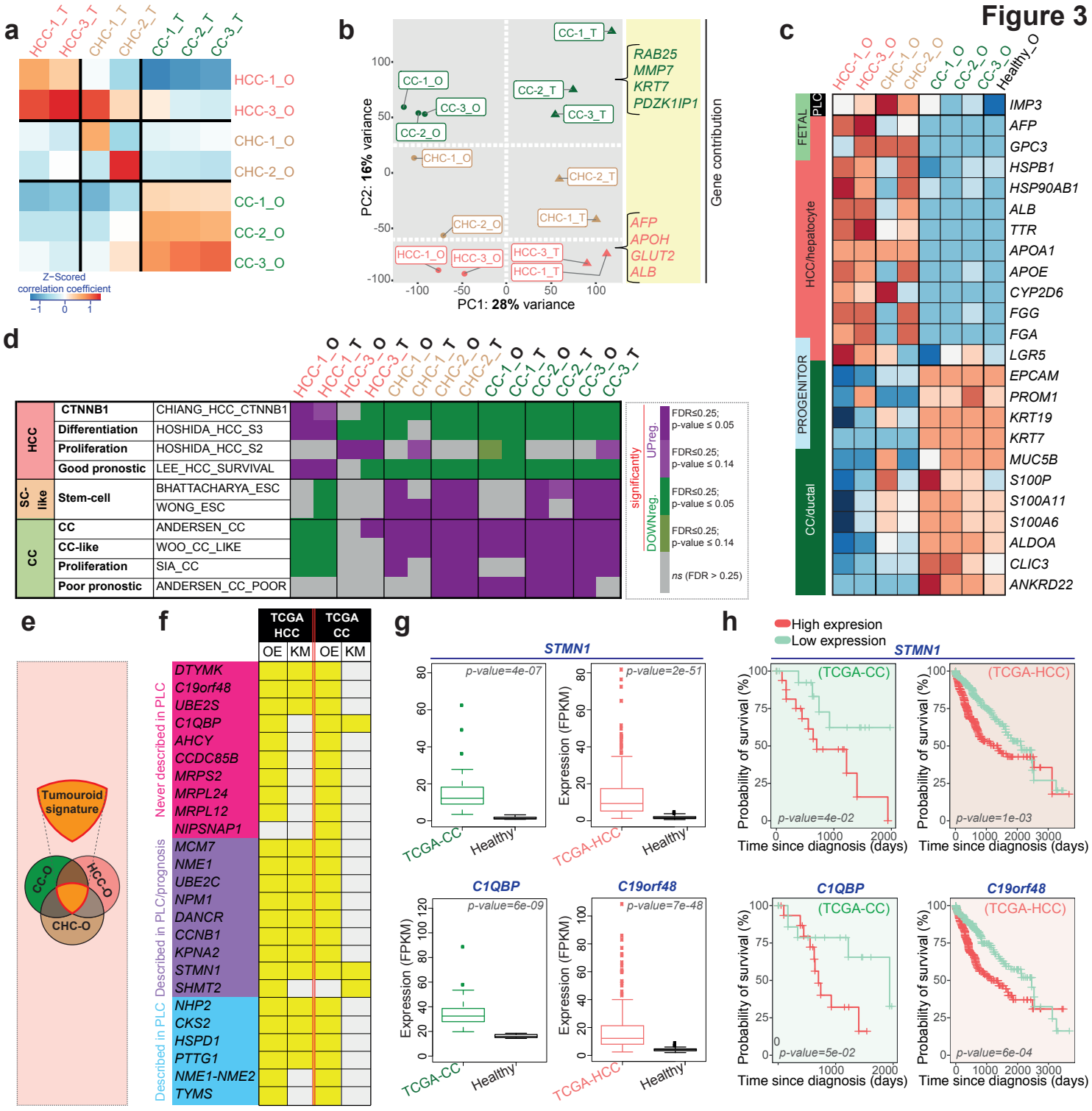

Figure 3: Genome wide gene expression analysis indicates that the tumouroids recapitulate the expression profile of the specific subtype of primary liver cancer (PLC) they were derived from and allow identifying potential new genes involved in PLC.
(a) Correlation heat map between PLC-tissue (_T) and paired PLC-derived organoid line (_O) expression profiles showing that the tumourigenic profile of the original tissue and specific subtype of PLC is maintained after long-term expansion in culture. Red, strong correlation; blue, low correlation. **(b)** PCA analysis showing samples plotted in 2 dimensions using their projections onto the first two principal components (PC1 and PC2). Each data point represents one sample, dot stands for tumouroids lines, triangle for PLC tissues. PC1 is strongly correlated with the type of sample (tumouroids vs tissue) whereas PC2 defines the 3 different PLC subtypes (HCC, CHC and CC). Of note, tumouroid lines and tissues are distributed consistently along PC2 according to their own PLC subtype. Some genes from the top 100 genes with highest loadings across PC2 are shown. **(c)** Heat map analysis of the log2 RPKM values (raw z-scored) of selected genes found highly expressed (red) in HCC and/or CHC and/or CC tumouroids. **(d)** Gene set enrichement analysis (GSEA) comparing the tumouroid lines' and associated tissues' gene expression signatures to 159 curated gene-sets associated with liver cancer and stem cell (representative plots shown in Suppl. Fig. 4). The heatmap shows some of the significantly UPregulated and DOWNregulated gene-sets (False discovery rate (FDR)<25%) in the tumouroid lines and paired tissues. Full list of gene-sets and significantly enriched gene-sets can be found in Suppl. dataset 2 and 3. **(e)** Schematic of the tumouroid signature. Venn diagram overlapping the upregulated genes in each tumouroid line compared to healthy organoids. **(f)** Table summarizing the results of the gene expression patterns (OE, overexpression) and outcome prediction (KM, Kaplan-Meier) analyses performed for the top genes of the tumouroid signature using publically available TCGA cohorts. The table details the p-values obtained for each analysis (OE in PLC, two-sided t-test ; KM analysis, log-rank test). p-value≤0.05 are defined as significant and color coded using yellow in the table. Only top the 25 genes are represented (Top 30 genes analysis and corresponding values can be found in Suppl. dataset 1). TCGA-HCC, 374 tumoural /50 normal samples; TCGA-CC, 31 tumoural /8 normal samples. **(g)** Box plots for the expression of *STMN1*, *C1QBP* and *C19orf48* in tumoural and normal tissues using the TCGA-HCC and/or CC cohorts. (h) Kaplan-Meier analyses in the TCGA-HCC and/or TCGA-CC cohorts based on the expression level of the gene of interest (*STMN1*, *C1QBP* and *C19orf48*) in the tumoural samples.

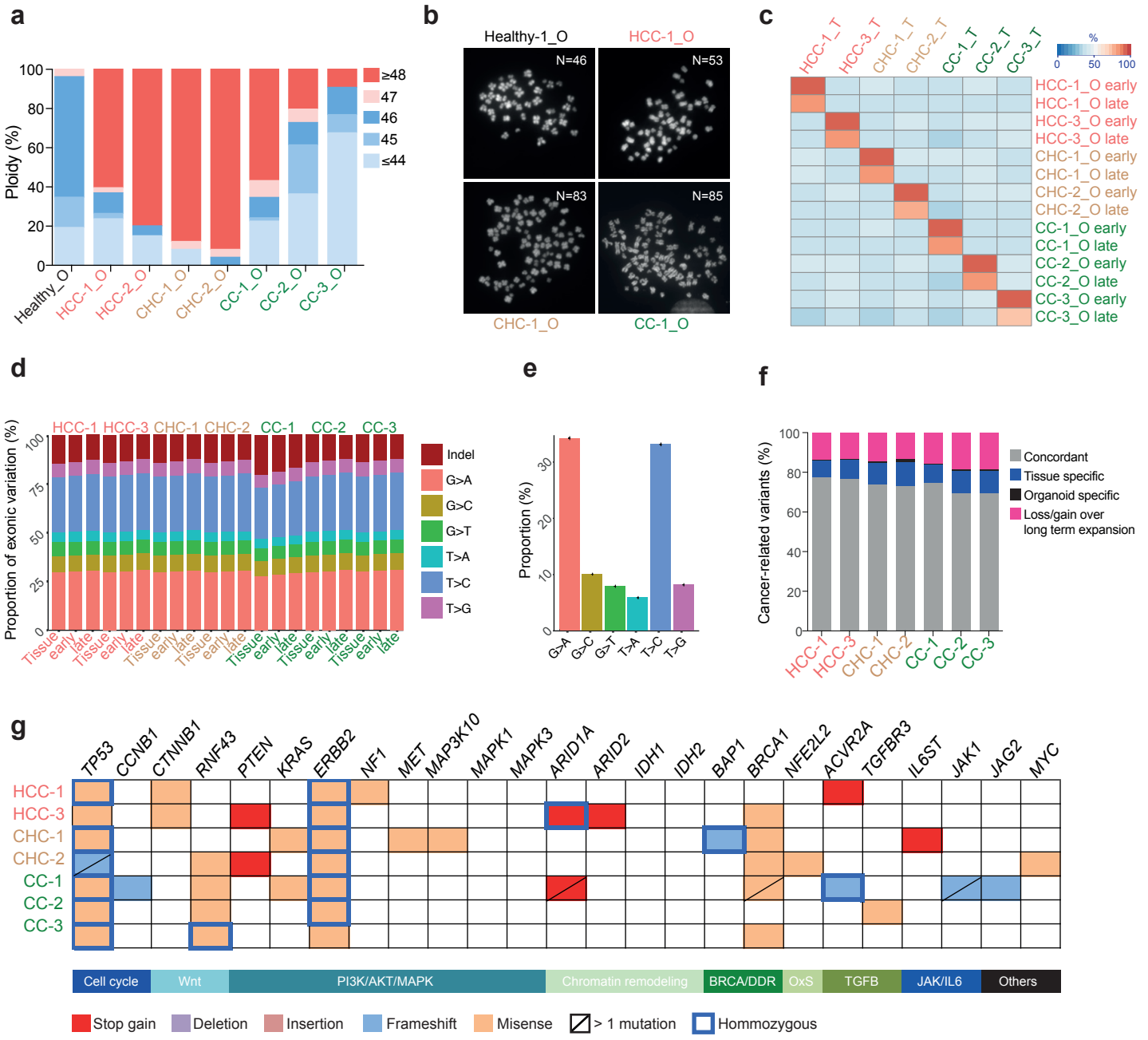

Figure 4: Tumouroids recapitulate the genetic alterations present in the patient's tumour.
(a) Ploidy analysis of tumouroid cultures expanded for at least 2 months in culture. Results are expressed as % of ploidy per number of metaphases counted (at least 25 total). Healthy-derived organoids were used as control. Experiment was performed at least in duplicate. **(b)** Representative images of organoid metaphases used for the ploidy analysis. **(c-g)** All somatic variants identified in all samples (21 total; 7 patients with 3 samples (Tissue/early organoid/late organoid)) were used for the global analyses after filtering for quality control as detailed in methods (c-e). For f-g, an additional filtering step was applied: a cancer related set of variants was defined by adding the following filtering steps: (1) SNVs, which were included in dbSNP were excluded, with the exception of those which were also included in COSMIC database (resultant variants are detailed in Fig. 4f and Suppl. Fig. 5b). (2) Synonymous SNVs were filtered out as were assumed to be unlikely involved in cancer. (3) A last filtering step was performed selecting for variants present in a panel of genes described in literature to be involved in cancer (847 cancer related genes total, for details see Suppl. Dataset 4). Resultant variants are provided in Suppl. Dataset 4 and were used to select relevant mutations described in Figure 5g. **(c)** Correlation heat-map between PLC-tissues (_T) and PLC-tumouroids (_O) variants identified. **(d)** Proportions of somatic variants across the samples, the 6 types of SNVs and the indels are represented. **(e)** Percentage of the 6 types of SNVs averaged across all samples (21 total; 7 patients with 3 samples (Tissue/early organoid/late organoid samples)). Graph represents mean±SD. **(f)** Bar plots indicate the concordance between the cancer related somatic variants identified in the tumour-of-origin and the corresponding tumouroids expanded for short or long term in culture. **(g)** Genes altered in tumouroid cultures and associated tissues and known to be mutated in liver OR gastrointestinal tumours. The type of mutation is indicated in the legend. OxS, oxidative stress.

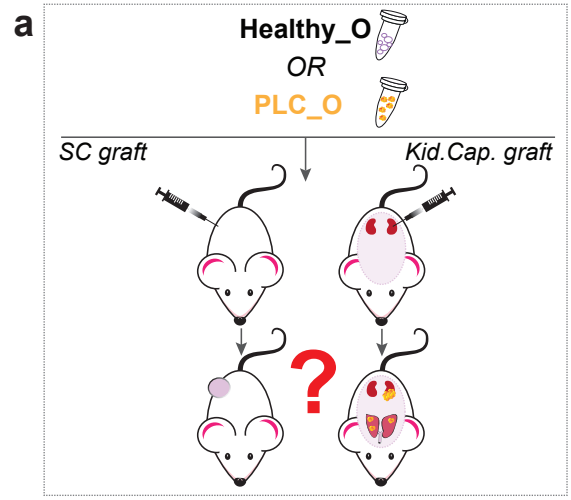

b

	Cells injected	Engraftment	Tumor	Efficiency
CC-1_O	1 000 000	SC	29/29	100%
HCC-1_O	1 000 000	SC	24/34	>70%
Healthy-1_O	1 000 000	SC	0/18	0%

c

	Cells injected	Engraftment	Tumor	Lung metastasis
CC-1_O	100 000	Kidney capsule	9/9	7/9
Healthy-1_O	100 000	Kidney capsule	0/6	0/6

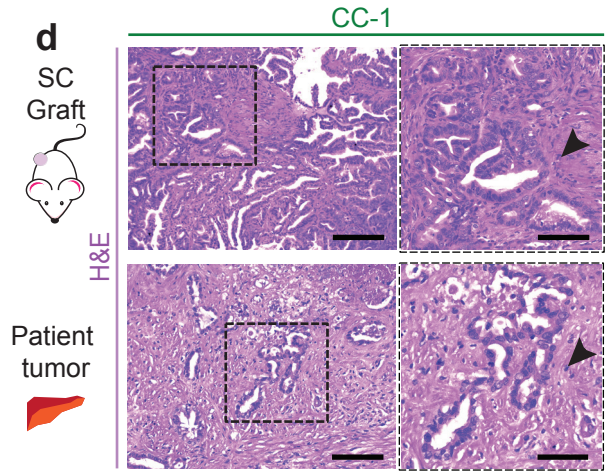

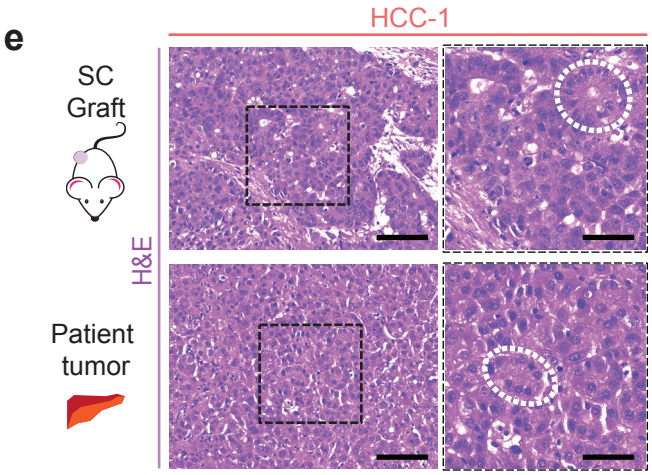

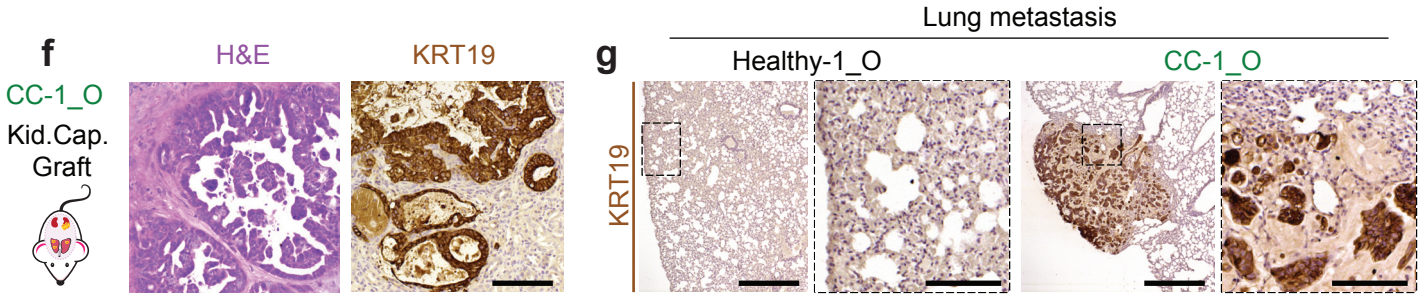

Figure 5: PLC tumouroids recapitulate patient's PLC tumour subtype and metastasis *in vivo* when transplanted in mice. **(a)** Experimental design. PLC tumouroids or Healthy liver-derived organoids expanded for >3 months in culture were transplanted subcutaneously (SC) or under the kidney capsule (Kid.Cap.) of immunocompromised NSG mice and analysed for the presence of tumour growth and metastasis following grafting. **(b-c)** Tables summarizing the number of cells, site of engraftment and analysis of tumour and lung metastasis. No tumour lesions were found in any of the mice receiving Healthy-1 organoids. Tumours were dissected at 1 (CC-1_O and Healthy-1_O) and 5 (HCC-1_O and Healthy-1_O) months (SC graft) and 0.5, 1, 2 and 3 months (Kid.Cap. graft) after injection. **(d)** Representative H&E staining of CC-1 tumouroids transplanted subcutaneously (top) into NSG mice and corresponding CC-1 patient's tumour sample (bottom). Note that the grafted CC-1 tumouroids tissue (top) recapitulates the histo-architecture of the patient's original tumour (bottom) including the extensive desmoplasia found on the CC-1 original sample (arrowheads). Scale bars, top left 250µm, top right 125µm, bottom left 125µm, and bottom right 62.5µm. **(e)** Representative H&E staining of HCC-1 tumouroids transplanted subcutaneously (top) into NSG mice and corresponding HCC-1 patient's tumour sample (bottom). Note that the grafted HCC-1 tumouroids tissue (top) recapitulates the histo-architecture of the patient's original tumour (bottom) including the pseudoglandullar rosettes, hallmark of HCC-1 original sample (dashed circle). Scale bars, left 125µm, right 62.5µm. **(f)** Representative H&E (left) and KRT19 (right) immunohistochemistry analyses of CC-1 tumouroids transplanted under the kidney capsule of NSG mice. Scale bars, 125µm. **(g)** Lung metastases derived from the human CC-1 tumouroids transplanted under the kidney capsule cells (right panels) were identified using a human specific KRT19 antibody. No metastases were found in the lungs of mice transplanted with Healthy-1 organoids (left panels). Scale bars, 500µm, magnification 125µm.

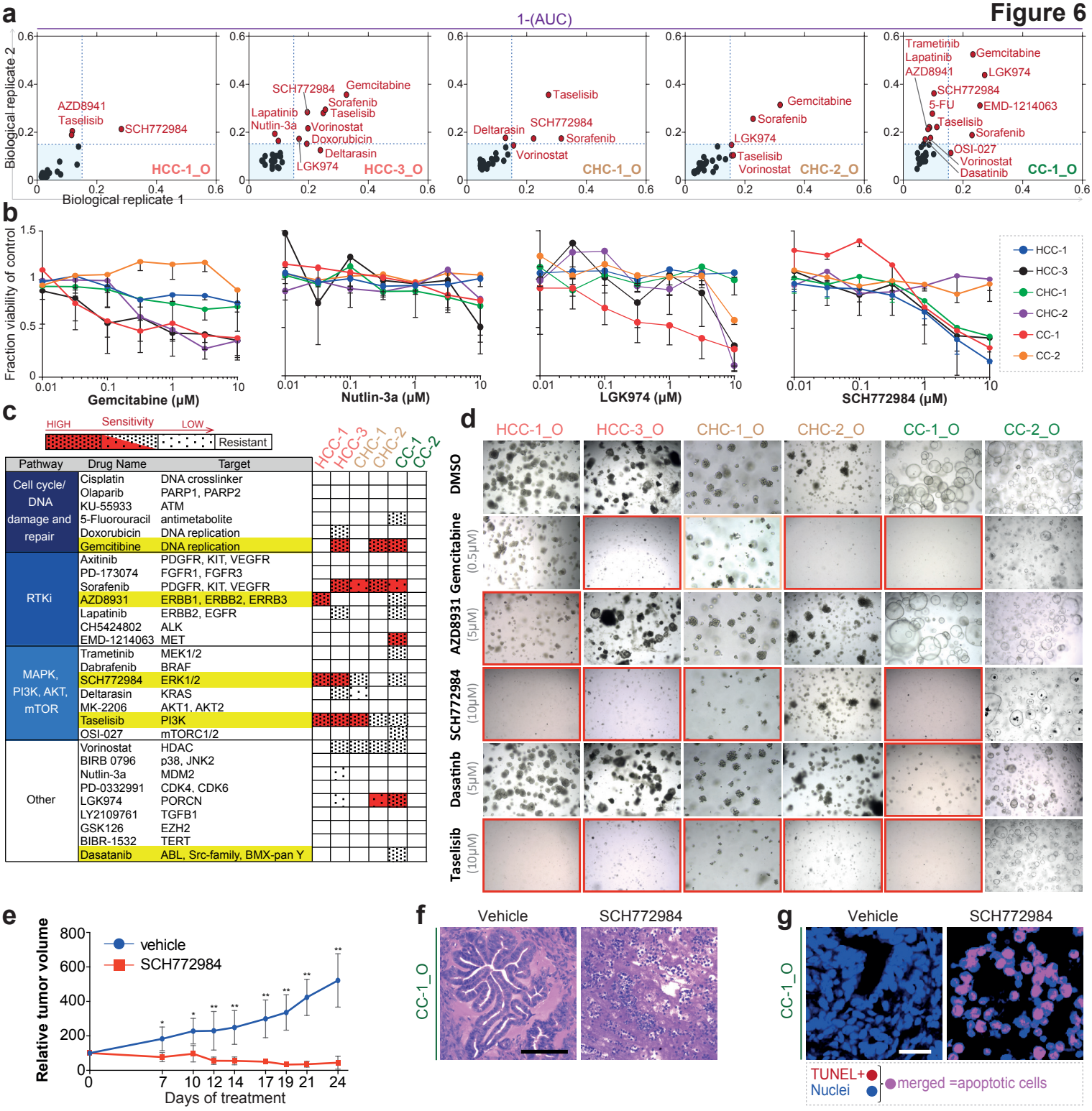

Pathway	Drug Name	Target
Cell cycle/ DNA damage and repair	Cisplatin	DNA crosslinker
	Olaparib	PARP1, PARP2
	KU-55933	ATM
	5-Fluorouracil	antimetabolite
	Doxorubicin	DNA replication
	Gemcitibine	DNA replication
RTKi	Axitinib	PDGFR, KIT, VEGFR
	PD-173074	FGFR1, FGFR3
	Sorafenib	PDGFR, KIT, VEGFR
	AZD8931	ERBB1, ERBB2, ERRB3
	Lapatinib	ERBB2, EGFR
	CH5424802	ALK
	EMD-1214063	MET
MAPK, PI3K, AKT, mTOR	Trametinib	MEK1/2
	Dabrafenib	BRAF
	SCH772984	ERK1/2
	Deltarasin	KRAS
	MK-2206	AKT1, AKT2
	Taselisib	PI3K
	OSI-027	mTORC1/2
Other	Vorinostat	HDAC
	BIRB 0796	p38, JNK2
	Nutlin-3a	MDM2
	PD-0332991	CDK4, CDK6
	LGK974	PORCN
	LY2109761	TGFB1
	GSK126	EZH2
	BIBR-1532	TERT
	Dasatanib	ABL, Src-family, BMX-pan Y

Figure 6: PLC tumouroid lines are a valuable resource for drug screening and allowed identification of ERK as a potential target for primary liver cancer.

(a) Scatterplot of 1-AUC values from two biological replicates of the drug screening data, highlighting drugs inducing a viability effect in five liver tumouroid lines. Each data point is the 1-AUC value for a given drug in a particular tumouroid line. **(b)** Dose-response curves after 6 days treatment with Gemcitabine, Nutlin-3a, LGK974 and SCH772984 generated from the luminescent signal intensities. Data displayed are average of the technical and biological replicates. **(c)** Summary of the different drugs used in the drug screening, the associated pathway and nominal targets and the screen results represented as a summary of the the 1-AUC and IC50 data generated for the different tumouroid lines. Red, IC50 within the screen range; Dense dotted pattern, 1-AUC>0.15 and dose response; scattered dotted pattern, 1-AUC>0.15 and sensitivity at highest value only. Compounds highlighted in yellow were selected for further validation. **(d)** Validation of viability effects of a subset of compounds using an organoid formation assay (see details in methods). **(e)** *In vivo* activity of SCH772984 in CC-1_O tumouroids grafted under the skin of NSG mice. Mice were treated with drug/vehicle twice daily for 20 days (n=5 in 2mg/kg of SCH772984 group, n=8 in vehicle group). From day 7 onwards, significant differences between the SCH772984 and the vehicle treated groups were observed. *, p-value<0.01; **, p-value<0.002 (Mann Whitney test, two-tailed). Results are shown as percentage of the tumour volume relative to day 0 (mean ±SD). **(f-g)** Histological analysis of the antitumor efficacy of SCH772984 on CC-1_O tumors was assessed 24 days after starting the treatment. Representative **(f)** H&E and **(g)** TUNEL staining performed on tissue sections from CC-1_O tumours treated with either vehicle (left) or SCH772984 (right). Representative images from 2 independent experiments are shown. Scale bar, 125μM (H&E) and 25μM (TUNEL).